
Momentum Centering and Asynchronous Update for Adaptive Gradient Methods

Juntang Zhuang¹; Yifan Ding²; Tommy Tang³; Nicha Dvornek¹;
 Sekhar Tatikonda¹; James S. Duncan¹

¹ Yale University; ² University of Central Florida; ³ University of Illinois at Urbana-Champaign
 {j.zhuang;nicha.dvornek;sekhar.tatikonda;james.duncan}@yale.edu;
 yf.ding@knights.ucf.edu;tommyt2@illinois.edu

Abstract

We propose ACProp (Asynchronous-centering-Prop), an adaptive optimizer which combines centering of second momentum and asynchronous update (e.g. for t -th update, denominator uses information up to step $t - 1$, while numerator uses gradient at t -th step). ACProp has both strong theoretical properties and empirical performance. With the example by Reddi et al. (2018), we show that asynchronous optimizers (e.g. AdaShift, ACProp) have weaker convergence condition than synchronous optimizers (e.g. Adam, RMSProp, AdaBelief); within asynchronous optimizers, we show that centering of second momentum further weakens the convergence condition. We demonstrate that ACProp has a convergence rate of $O(\frac{1}{\sqrt{T}})$ for the stochastic non-convex case, which matches the oracle rate and outperforms the $O(\frac{\log T}{\sqrt{T}})$ rate of RMSProp and Adam. We validate ACProp in extensive empirical studies: ACProp outperforms both SGD and other adaptive optimizers in image classification with CNN, and outperforms well-tuned adaptive optimizers in the training of various GAN models, reinforcement learning and transformers. To sum up, ACProp has good theoretical properties including weak convergence condition and optimal convergence rate, and strong empirical performance including good generalization like SGD and training stability like Adam. We provide the implementation at <https://github.com/juntang-zhuang/ACProp-Optimizer>.

1 Introduction

Deep neural networks are typically trained with first-order gradient optimizers due to their computational efficiency and good empirical performance [1]. Current first-order gradient optimizers can be broadly categorized into the stochastic gradient descent (SGD) [2] family and the adaptive family. The SGD family uses a global learning rate for all parameters, and includes variants such as Nesterov-accelerated SGD [3], SGD with momentum [4] and the heavy-ball method [5]. Compared with the adaptive family, SGD optimizers typically generalize better but converge slower, and are the default for vision tasks such as image classification [6], object detection [7] and segmentation [8].

The adaptive family uses element-wise learning rate, and the representatives include AdaGrad [9], AdaDelta [10], RMSProp [11], Adam [12] and its variants such as AdamW [13], AMSGrad [14] AdaBound [15], AdaShift [16], Padam [30], RAdam [17] and AdaBelief [18]. Compared with the SGD family, the adaptive optimizers typically converge faster and are more stable, hence are the default for generative adversarial networks (GANs) [19], transformers [20], and deep reinforcement learning [21].

We broadly categorize adaptive optimizers according to different criteria, as in Table. 1. (a) *Centered v.s. uncentered* Most optimizers such as Adam and AdaDelta uses uncentered second momentum in

Table 1: Categories of adaptive optimizers

	Uncentered second momentum	Centered second momentum
Synchronous	Adam, RAdam, AdaDelta, RMSProp, Padam	RMSProp-center, SDProp, AdaBelief
Asynchronous	AdaShift	ACProp (ours)

the denominator; RMSProp-center [11], SDProp [22] and AdaBelief [18] use square root of centered second momentum in the denominator. AdaBelief [18] is shown to achieve good generalization like the SGD family, fast convergence like the adaptive family, and training stability in complex settings such as GANs. (b) *Sync vs async* The synchronous optimizers typically use gradient g_t in both numerator and denominator, which leads to correlation between numerator and denominator; most existing optimizers belong to this category. The asynchronous optimizers decorrelate numerator and denominator (e.g. by using g_t as numerator and use $\{g_0, \dots, g_{t-1}\}$ in denominator for the t -th update), and is shown to have weaker convergence conditions than synchronous optimizers [16].

We propose Asynchronous Centering Prop (ACProp), which combines centering of second momentum with the asynchronous update. We show that ACProp has both good theoretical properties and strong empirical performance. Our contributions are summarized as below:

- **Convergence condition** (a) *Async vs Sync* We show that for the example by Reddi et al. (2018), asynchronous optimizers (AdaShift, ACProp) converge for any valid hyper-parameters, while synchronous optimizers (Adam, RMSProp et al.) could diverge if the hyper-parameters are not carefully chosen. (b) *Async-Center vs Async-Uncenter* Within the asynchronous optimizers family, by example of an online convex problem with sparse gradients, we show that Async-Center (ACProp) has weaker conditions for convergence than Async-Uncenter (AdaShift).
- **Convergence rate** We demonstrate that ACProp achieves a convergence rate of $O(\frac{1}{\sqrt{T}})$ for stochastic non-convex problems, matching the oracle of first-order optimizers [23], and outperforms the $O(\frac{\log T}{\sqrt{T}})$ rate of Adam and RMSProp.
- **Empirical performance** We validate performance of ACProp in experiments: on image classification tasks, ACProp outperforms SGD and AdaBelief, and demonstrates good generalization performance; in experiments with transformer, reinforcement learning and various GAN models, ACProp outperforms well-tuned Adam, demonstrating high stability. ACProp often outperforms AdaBelief, and achieves good generalization like SGD and training stability like Adam.

2 Overview of algorithms

2.1 Notations

- $x, x_t \in \mathbb{R}^d$: x is a d -dimensional parameter to be optimized, and x_t is the value at step t .
- $f(x), f^* \in \mathbb{R}$: $f(x)$ is the scalar-valued function to be minimized, with optimal (minimal) f^* .
- $\alpha_t, \epsilon \in \mathbb{R}$: α_t is the learning rate at step t . ϵ is a small number to avoid division by 0.
- $g_t \in \mathbb{R}^d$: The noisy observation of gradient $\nabla f(x_t)$ at step t .
- $\beta_1, \beta_2 \in \mathbb{R}$: Constants for exponential moving average, $0 \leq \beta_1, \beta_2 < 1$.
- $m_t \in \mathbb{R}^d$: $m_t = \beta_1 m_{t-1} + (1 - \beta_1) g_t$. The Exponential Moving Average (EMA) of observed gradient at step t .
- $\Delta g_t \in \mathbb{R}^d$: $\Delta g_t = g_t - m_t$. The difference between observed gradient g_t and EMA of g_t .
- $v_t \in \mathbb{R}^d$: $v_t = \beta_2 v_{t-1} + (1 - \beta_2) g_t^2$. The EMA of g_t^2 .
- $s_t \in \mathbb{R}^d$: $s_t = \beta_2 s_{t-1} + (1 - \beta_2) (\Delta g_t)^2$. The EMA of $(\Delta g_t)^2$.

2.2 Algorithms

In this section, we summarize the AdaBelief [18] method in Algo. 1 and ACProp in Algo. 2. For the ease of notations, all operations in Algo. 1 and Algo. 2 are element-wise, and we omit the bias-correction step of m_t and s_t for simplicity. $\Pi_{\mathcal{F}}$ represents the projection onto feasible set \mathcal{F} .

Algorithm 1: AdaBelief

Initialize $x_0, m_0 \leftarrow 0, s_0 \leftarrow 0, t \leftarrow 0$
While x_t not converged
 $t \leftarrow t + 1$
 $g_t \leftarrow \nabla_x f_t(x_{t-1})$
 $m_t \leftarrow \beta_1 m_{t-1} + (1 - \beta_1) g_t$
 $s_t \leftarrow \beta_2 s_{t-1} + (1 - \beta_2) (g_t - m_t)^2$
 $x_t \leftarrow \prod_{\mathcal{F}, \sqrt{s_t}} \left(x_{t-1} - \frac{\alpha}{\sqrt{s_t + \epsilon}} m_t \right)$

Algorithm 2: ACProp

Initialize $x_0, m_0 \leftarrow 0, s_0 \leftarrow 0, t \leftarrow 0$
While x_t not converged
 $t \leftarrow t + 1$
 $g_t \leftarrow \nabla_x f_t(x_{t-1})$
 $m_t \leftarrow \beta_1 m_{t-1} + (1 - \beta_1) g_t$
 $x_t \leftarrow \prod_{\mathcal{F}, \sqrt{s_{t-1}}} \left(x_{t-1} - \frac{\alpha}{\sqrt{s_{t-1} + \epsilon}} g_t \right)$
 $s_t \leftarrow \beta_2 s_{t-1} + (1 - \beta_2) (g_t - m_t)^2$

We first introduce the notion of “sync (async)” and “center (uncenter)”. (a) *Sync vs Async* The update on parameter x_t can be generally split into a numerator (e.g. m_t, g_t) and a denominator (e.g. $\sqrt{s_t}, \sqrt{v_t}$). We call it “sync” if the denominator depends on g_t , such as in Adam and RMSProp; and call it “async” if the denominator is independent of g_t , for example, denominator uses information up to step $t - 1$ for the t -th step. (b) *Center vs Uncenter* The “uncentered” update uses v_t , the exponential moving average (EMA) of g_t^2 ; while the “centered” update uses s_t , the EMA of $(g_t - m_t)^2$.

Adam (Sync-Uncenter) The Adam optimizer [12] stores the EMA of the gradient in m_t , and stores the EMA of g_t^2 in v_t . For each step of the update, Adam performs element-wise division between m_t and $\sqrt{v_t}$. Therefore, the term $\alpha_t \frac{1}{\sqrt{v_t}}$ can be viewed as the element-wise learning rate. Note that β_1 and β_2 are two scalars controlling the smoothness of the EMA for the first and second moment, respectively. When $\beta_1 = 0$, Adam reduces to RMSProp [24].

AdaBelief (Sync-Center) AdaBelief optimizer [18] is summarized in Algo. 1. Compared with Adam, the key difference is that it replaces the uncentered second moment v_t (EMA of g_t^2) by an estimate of the centered second moment s_t (EMA of $(g_t - m_t)^2$). The intuition is to view m_t as an estimate of the expected gradient: if the observation g_t deviates much from the prediction m_t , then it takes a small step; if the observation g_t is close to the prediction m_t , then it takes a large step.

AdaShift (Async-Uncenter) AdaShift [16] performs temporal decorrelation between numerator and denominator. It uses information of $\{g_{t-n}, \dots, g_t\}$ for the numerator, and uses $\{g_0, \dots, g_{t-n-1}\}$ for the denominator, where n is the “delay step” controlling where to split sequence $\{g_i\}_{i=0}^t$. The numerator is independent of denominator because each g_i is only used in either numerator or denominator.

ACProp (Async-Center) Our proposed ACProp is the asynchronous version of AdaBelief and is summarized in Algo. 2. Compared to AdaBelief, the key difference is that ACProp uses s_{t-1} in the denominator for step t , while AdaBelief uses s_t . Note that s_t depends on g_t , while s_{t-1} uses history up to step $t - 1$. This modification is important to ensure that $\mathbb{E}(g_t / \sqrt{s_{t-1}} | g_0, \dots, g_{t-1}) = (\mathbb{E}g_t) / \sqrt{s_{t-1}}$. It’s also possible to use a delay step larger than 1 similar to AdaShift, for example, use $EMA(\{g_i\}_{i=t-n}^t)$ as numerator, and $EMA(\{(g_i - m_i)^2\}_{i=0}^{t-n-1})$ for denominator.

3 Analyze the conditions for convergence

We analyze the convergence conditions for different methods in this section. We first analyze the counter example by Reddi et al. (2018) and show that async-optimizers (AdaShift, ACProp) always converge $\forall \beta_1, \beta_2 \in (0, 1)$, while sync-optimizers (Adam, AdaBelief, RMSProp et al.) would diverge if (β_1, β_2) are not carefully chosen; hence, async-optimizers have weaker convergence conditions than sync-optimizers. Next, we compare async-uncenter (AdaShift) with async-center (ACProp) and show that momentum centering further weakens the convergence condition for sparse-gradient problems. Therefore, ACProp has weaker convergence conditions than AdaShift and other sync-optimizers.

3.1 Sync vs Async

We show that for the example in [14], async-optimizers (ACProp, AdaShift) have weaker convergence conditions than sync-optimizers (Adam, RMSProp, AdaBelief).

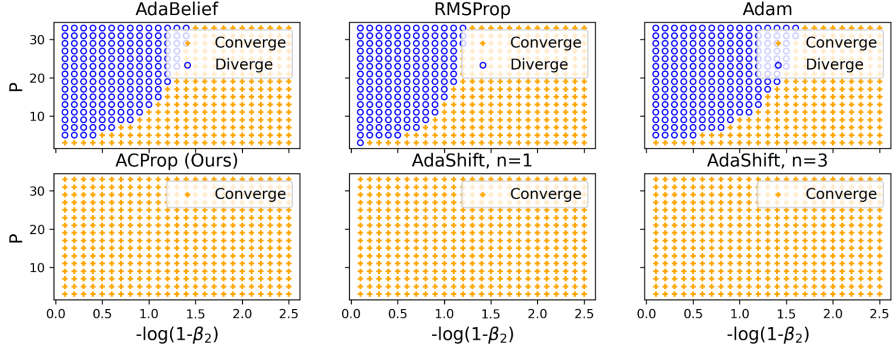


Figure 1: Numerical results for the example defined by Eq. (1). We set the initial value as $x_0 = 0$, and run each optimizer for 10^4 steps trying different initial learning rates in $\{10^{-5}, 10^{-4}, 10^{-3}, 10^{-2}, 10^{-1}, 1.0\}$, and set the learning rate decays with $1/\sqrt{t}$. If there’s a proper initial learning rate, such that the average distance between the parameter and its optimal value $x^* = -1$ for the last 1000 steps is below 0.01, then it’s marked as “converge” (orange plus symbol), otherwise as “diverge” (blue circle). For each optimizer, we sweep through different β_2 values in a log grid (x -axis), and sweep through different values of P in the definition of problem (y -axis). We plot the result for $\beta_1 = 0.9$ here; for results with different β_1 values, please refer to appendix. Our results indicate that in the (P, β_2) plane, there’s a threshold curve beyond which sync-optimizers (Adam, RMSProp, AdaBelief) will diverge; however, async-optimizers (ACProp, AdaShift) always converge for any point in the (P, β_2) plane. Note that for AdaShift, a larger delay step n is possible to cause divergence (see example in Fig. 2 with $n = 10$). To validate that the “divergence” is not due to numerical issues and sync-optimizers are drifting away from optimal, we plot trajectories in Fig. 2

Lemma 3.1 (Thm.1 in [14]). *There exists an online convex optimization problem where sync-optimizers (e.g. Adam, RMSProp) have non-zero average regret, and one example is*

$$f_t(x) = \begin{cases} Px, & \text{if } t \% P = 1 \\ -x, & \text{Otherwise} \end{cases} \quad x \in [-1, 1], P \in \mathbb{N}, P \geq 3 \quad (1)$$

Lemma 3.2 ([25]). *For problem (1) with any fixed P , there’s a threshold of β_2 above which RMSProp converges.*

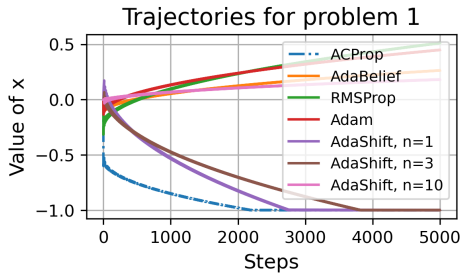


Figure 2: Trajectories of x for different optimizers in Problem by Eq. 1. Initial point is $x_0 = 0$, the optimal is $x^* = -1$, the trajectories show that sync-optimizers (Adam, AdaBelief, RMSProp) diverge from the optimal, validating the divergent area in Fig. 1 is correct rather than artifacts of numerical issues. Async-optimizers (ACProp, AdaShift) converge to optimal value, but large delay step n in AdaShift could cause non-convergence.

Lemma. 3.1 tells half of the story: looking at each vertical line in the subfigure of Fig. 1, that is, for each fixed hyper-parameter β_2 , there exists sufficiently large P such that Adam (and RMSProp) would diverge. Lemma. 3.2 tells the other half of the story: looking at each horizontal line in the subfigure of Fig. 1, for each problem with a fixed period P , there exists sufficiently large β_2 s beyond which Adam can converge.

The complete story is to look at the (P, β_2) plane in Fig. 1. There is a boundary between convergence and divergence area for sync-optimizers (Adam, RMSProp, AdaBelief), while async-optimizers (ACProp, AdaShift) always converge.

Lemma 3.3. *For the problem defined by Eq. (1), using learning rate schedule of $\alpha_t = \frac{\alpha_0}{\sqrt{t}}$, async-optimizers (ACProp and AdaShift with $n = 1$) always converge $\forall \beta_1, \beta_2 \in (0, 1), \forall P \in \mathbb{N}, P \geq 3$.*

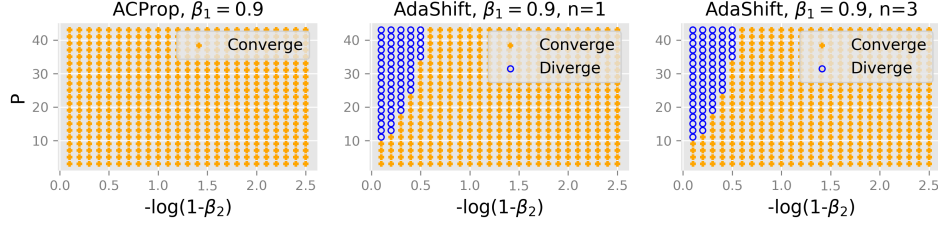


Figure 3: Area of convergence for the problem in Eq. (2). The numerical experiment is performed under the same setting as in Fig. 1. Our results experimentally validated the claim that compared with async-uncenter (AdaShift), async-center (ACProp) has a larger convergence area in the hyper-parameter space.

The proof is in the appendix. Note that for AdaShift, proof for the always-convergence property only holds when $n = 1$; larger n could cause divergence (e.g. $n = 10$ causes divergence as in Fig. 2). The always-convergence property of ACProp and AdaShift comes from the un-biased stepsize, while the stepsize for sync-optimizers are biased due to correlation between numerator and denominator. Taking RMSProp as example of sync-optimizer, the update is $-\alpha_t \frac{g_t}{\sqrt{v_t}} = -\alpha_t \frac{g_t}{\sqrt{\beta_2 g_0^2 + \dots + \beta_2 g_{t-1}^2 + g_t^2}}$.

Note that g_t is used both in the numerator and denominator, hence a large g_t does not necessarily generate a large stepsize. For the example in Eq. (1), the optimizer observes a gradient of -1 for $P - 1$ times and a gradient of P once; due to the biased stepsize in sync-optimizers, the gradient of P does not generate a sufficiently large stepsize to compensate for the effect of wrong gradients -1 , hence cause non-convergence. For async-optimizers, g_t is not used in the denominator, therefore, the stepsize is not biased and async-optimizers has the always-convergence property.

Remark Reddi et al. (2018) proposed AMSGrad to track the element-wise maximum of v_t in order to achieve the always-convergence property. However, tracking the maximum in the denominator will in general generate a small stepsize, which often harms empirical performance. We demonstrate this through experiments in later sections in Fig. 6.

3.2 Async-Uncenter vs Async-Center

In the last section, we demonstrated that async-optimizers have weaker convergence conditions than sync-optimizers. In this section, within the async-optimizer family, we analyze the effect of centering second momentum. We show that compared with async-uncenter (AdaShift), async-center (ACProp) has weaker convergence conditions. We consider the following online convex problem:

$$f_t(x) = \begin{cases} P/2 \times x, & t \% P == 1 \\ -x, & t \% P == P - 2 \\ 0, & \text{otherwise} \end{cases} \quad P > 3, P \in \mathbb{N}, x \in [0, 1]. \quad (2)$$

Initial point is $x_0 = 0.5$. Optimal point is $x^* = 0$. We have the following results:

Lemma 3.4. *For the problem defined by Eq. (2), consider the hyper-parameter tuple (β_1, β_2, P) , there exists cases where ACProp converges but AdaShift with $n = 1$ diverges, but not vice versa.*

We provide the proof in the appendix. Lemma. 3.4 implies that ACProp has a larger area of convergence than AdaShift, hence the centering of second momentum further weakens the convergence conditions. We first validate this claim with numerical experiments in Fig. 3; for sanity check, we plot the trajectories of different optimizers in Fig. 4. We observe that the convergence of AdaShift is influenced by delay step n , and there's no good criterion to select a good value of n , since Fig. 2 requires a small n for convergence in problem (1), while Fig. 4 requires a large n for convergence in problem (2). ACProp has a larger area of convergence, indicating that both async update and second momentum centering helps weaken the convergence conditions.

We provide an intuitive explanation on why momentum centering helps convergence. Due to the periodicity of the problem, the optimizer behaves almost periodically as $t \rightarrow \infty$. Within each period, the optimizer observes one positive gradient $P/2$ and one negative gradient -1 . As in Fig. 5, between observing non-zero gradients, the gradient is always 0. Within each period, ACprop will perform a positive update $P/(2\sqrt{s^+})$ and a negative update $-1/\sqrt{s^-}$, where s^+ (s^-) is the value of denominator before observing positive (negative) gradient. Similar notations for v^+ and v^- in AdaShift. A net update in the correct direction requires $\frac{P}{2\sqrt{s^+}} > \frac{1}{\sqrt{s^-}}$, (or $s^+/s^- < P^2/4$).

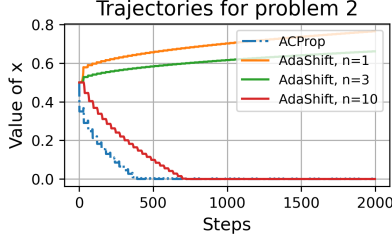


Figure 4: Trajectories for problem defined by Eq. (2). Note that the optimal point is $x^* = 0$.

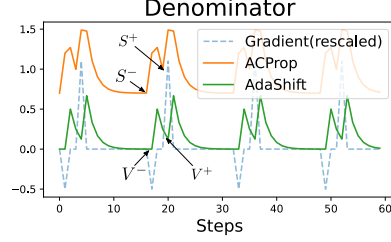


Figure 5: Value of uncentered second momentum v_t and centered momentum s_t for problem (2).

When observing 0 gradient, for AdaShift, $v_t = \beta_2 v_{t-1} + (1 - \beta_2)0^2$; for ACProp, $s_t = \beta_2 s_{t-1} + (1 - \beta_2)(0 - m_t)^2$ where $m_t \neq 0$. Therefore, v^- decays exponentially to 0, but s^- decays to a non-zero constant, hence $\frac{s^+}{s^-} < \frac{v^+}{v^-}$, hence ACProp is easier to satisfy $s^+/s^- < P^2/4$ and converge.

4 Analysis on convergence rate

In this section, we show that ACProp converges at a rate of $O(1/\sqrt{T})$ in the stochastic nonconvex case, which matches the oracle [23] for first-order optimizers and outperforms the $O(\log T/\sqrt{T})$ rate for sync-optimizers (Adam, RMSProp and AdaBelief) [26, 25, 18]. We further show that the upper bound on regret of async-center (ACProp) outperforms async-uncenter (AdaShift) by a constant.

For the ease of analysis, we denote the update as: $x_t = x_{t-1} - \alpha_t A_t g_t$, where A_t is the diagonal preconditioner. For SGD, $A_t = I$; for sync-optimizers (RMSProp), $A_t = \frac{1}{\sqrt{v_t + \epsilon}}$; for AdaShift with $n = 1$, $A_t = \frac{1}{\sqrt{v_{t-1} + \epsilon}}$; for ACProp, $A_t = \frac{1}{\sqrt{s_{t-1} + \epsilon}}$. For async optimizers, $\mathbb{E}[A_t g_t | g_0, \dots, g_{t-1}] = A_t \mathbb{E}g_t$; for sync-optimizers, this does not hold because g_t is used in A_t

Theorem 4.1 (convergence for stochastic non-convex case). *Under the following assumptions:*

- f is continuously differentiable, f is lower-bounded by f^* and upper bounded by M_f . $\nabla f(x)$ is globally Lipschitz continuous with constant L :

$$\|\nabla f(x) - \nabla f(y)\| \leq L\|x - y\| \quad (3)$$

- For any iteration t , g_t is an unbiased estimator of $\nabla f(x_t)$ with variance bounded by σ^2 . Assume norm of g_t is bounded by M_g .

$$\mathbb{E}[g_t] = \nabla f(x_t) \quad \mathbb{E}[|g_t - \nabla f(x_t)|^2] \leq \sigma^2 \quad (4)$$

then for $\beta_1, \beta_2 \in [0, 1)$, with learning rate schedule as: $\alpha_t = \alpha_0 t^{-\eta}$, $\alpha_0 \leq \frac{C_l}{LC_u^2}$, $\eta \in [0.5, 1)$ for the sequence $\{x_t\}$ generated by ACProp, we have

$$\frac{1}{T} \sum_{t=1}^T \|\nabla f(x_t)\|^2 \leq \frac{2}{C_l} \left[(M_f - f^*)\alpha_0 T^{\eta-1} + \frac{LC_u^2 \sigma^2 \alpha_0}{2(1-\eta)} T^{-\eta} \right] \quad (5)$$

where C_l and C_u are scalars representing the lower and upper bound for A_t , e.g. $C_l I \preceq A_t \preceq C_u I$, where $A \preceq B$ represents $B - A$ is semi-positive-definite.

Note that there's a natural bound for C_l and C_u : $C_u \leq \frac{1}{\epsilon}$ and $C_l \geq \frac{1}{2M_g}$ because ϵ is added to denominator to avoid division by 0, and g_t is bounded by M_g . Thm. 4.1 implies that ACProp has a convergence rate of $O(1/\sqrt{T})$ when $\eta = 0.5$; equivalently, in order to have $\|\nabla f(x)\|^2 \leq \delta^2$, ACProp requires at most $O(\delta^{-4})$ steps.

Theorem 4.2 (Oracle complexity [23]). *For a stochastic non-convex problem satisfying assumptions in Theorem 4.1, using only up to first-order gradient information, in the worst case any algorithm requires at least $O(\delta^{-4})$ queries to find a δ -stationary point x such that $\|\nabla f(x)\|^2 \leq \delta^2$.*

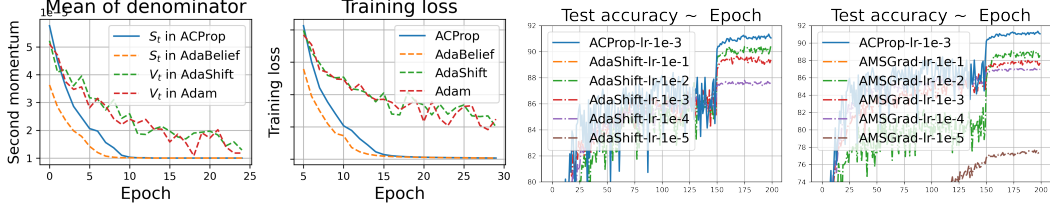


Figure 6: From left to right: (a) Mean value of denominator for a 2-layer MLP on MNIST dataset. (b) Training loss of different optimizers for the 2-layer MLP model. (c) Performance of AdaShift for VGG-11 on CIFAR10 varying with learning rate ranging from 1e-1 to 1e-5, we plot the performance of ACProp with learning rate 1e-3 as reference. Missing lines are because their accuracy are below display threshold. All methods decay learning rate by a factor of 10 at 150th epoch. (d) Performance of AMSGrad for VGG-11 on CIFAR10 varying with learning rate under the same setting in (c).

Optimal rate in big O Thm. 4.1 and Thm. 4.2 imply that async-optimizers achieves a convergence rate of $O(1/\sqrt{T})$ for the stochastic non-convex problem, which matches the oracle complexity and outperforms the $O(\log T/\sqrt{T})$ rate of sync-optimizers (Adam [14], RMSProp[25], AdaBelief [18]). Adam and RMSProp are shown to achieve $O(1/\sqrt{T})$ rate under the stricter condition that $\beta_{2,t} \rightarrow 1$ [27]. A similar rate has been achieved in AVAGrad [28], and AdaGrad is shown to achieve a similar rate [29]. Despite the same convergence rate, we show that ACProp has better empirical performance.

Constants in the upper bound of regret Though both async-center and async-uncenter optimizers have the same convergence rate with matching upper and lower bound in big O notion, the constants of the upper bound on regret is different. Thm. 4.1 implies that the upper bound on regret is an increasing function of $1/C_l$ and C_u , and

$$1/C_l = \sqrt{K_u} + \epsilon, \quad C_u = 1/(\sqrt{K_l} + \epsilon)$$

where K_l and K_u are the lower and upper bound of second momentum, respectively.

We analyze the constants in regret by analyzing K_l and K_u . If we assume the observed gradient g_t follows some independent stationary distribution, with mean μ and variance σ^2 , then approximately

$$\text{Uncentered second momentum: } 1/C_l^v = \sqrt{K_u^v} + \epsilon \approx \sqrt{\mu^2 + \sigma^2} + \epsilon \quad (6)$$

$$\text{Centered second momentum: } 1/C_l^s = \sqrt{K_u^s} + \epsilon \approx \sqrt{\sigma^2} + \epsilon \quad (7)$$

During early phase of training, in general $|\mu| \gg \sigma$, hence $1/C_l^s \ll 1/C_l^v$, and the centered version (ACProp) can converge faster than uncentered type (AdaShift) by a constant factor of around $\frac{\sqrt{\mu^2 + \sigma^2} + \epsilon}{\sqrt{\sigma^2} + \epsilon}$. During the late phase, g_t is centered around 0, and $|\mu| \ll \sigma$, hence K_l^v (for uncentered version) and K_l^s (for centered version) are both close to 0, hence C_u term is close for both types.

Remark We emphasize that ACProp rarely encounters numerical issues caused by a small s_t as denominator, even though Eq. (7) implies a lower bound for s_t around σ^2 which could be small in extreme cases. Note that s_t is an estimate of mixture of two aspects: the change in true gradient $\|\nabla f_t(x) - \nabla f_{t-1}(x)\|^2$, and the noise in g_t as an observation of $\nabla f(x)$. Therefore, two conditions are essential to achieve $s_t = 0$: the true gradient $\nabla f_t(x)$ remains constant, and g_t is a noise-free observation of $\nabla f_t(x)$. Eq. (7) is based on assumption that $\|\nabla f_t(x) - \nabla f_{t-1}(x)\|^2 = 0$, if we further assume $\sigma = 0$, then the problem reduces to a trivial ideal case: a linear loss surface with clean observations of gradient, which is rarely satisfied in practice. More discussions are in appendix.

Empirical validations We conducted experiments on the MNIST dataset using a 2-layer MLP. We plot the average value of v_t for uncentered-type and s_t for centered-type optimizers; as Fig. 6(a,b) shows, we observe $s_t \leq v_t$ and the centered-type (ACProp, AdaBelief) converges faster, validating our analysis for early phases. For epochs > 10 , we observe that $\min s_t \approx \min v_t$, validating our analysis for late phases.

As in Fig. 6(a,b), the ratio v_t/s_t decays with training, and in fact it depends on model structure and dataset noise. Therefore, empirically it's hard to compensate for the constants in regret by applying a larger learning rate for async-uncenter optimizers. As shown in Fig. 6(c,d), for VGG network on CIFAR10 classification task, we tried different initial learning rates for AdaShift (async-uncenter) and AMSGrad ranging from 1e-1 to 1e-5, and their performances are all inferior to ACProp with a learning rate 1e-3. Please see Fig.8 for a complete table varying with hyper-parameters.

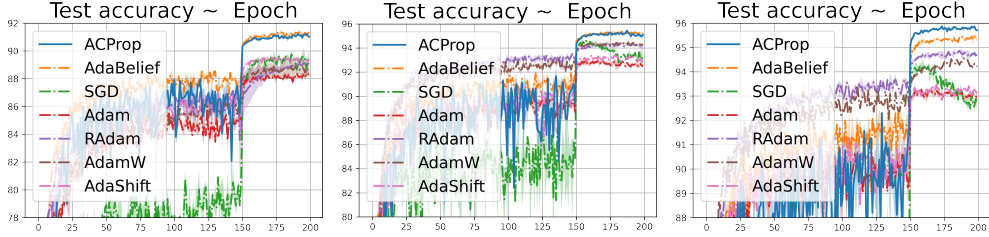


Figure 7: Test accuracy (*mean ± std*) on CIFAR10 dataset. Left to right: VGG-11, ResNet-34, DenseNet-121.

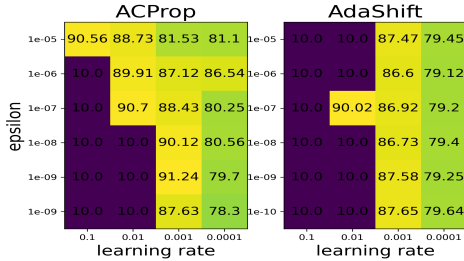


Figure 8: Test accuracy (%) of VGG network on CIFAR10 under different hyper-parameters. We tested learning rate in $\{10^{-1}, 10^{-2}, 10^{-3}, 10^{-4}\}$ and $\epsilon \in \{10^{-5}, \dots, 10^{-9}\}$.

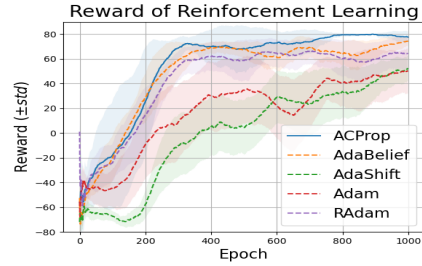


Figure 9: The reward (higher is better) curve of a DQN-network on the four-rooms problem. We report the mean and standard deviation across 10 independent runs.

Table 2: Top-1 accuracy of ResNet18 on ImageNet. \diamond is reported in PyTorch Documentation, \dagger is reported in [?], * is reported in [17], \ddagger is reported in [18]

	SGD	Padam	Adam	AdamW	RAdam	AdaShift	AdaBelief	ACProp
	69.76 \diamond (70.23 \dagger)	70.07 \dagger	66.54*	67.93 \dagger	67.62*	65.28	70.08 \ddagger	70.46

5 Experiments

We validate the performance of ACProp in various experiments, including image classification with convolutional neural networks (CNN), reinforcement learning with deep Q-network (DQN), machine translation with transformer and generative adversarial networks (GANs). We aim to test both the generalization performance and training stability: SGD family optimizers typically are the default for CNN models such as in image recognition [6] and object detection [7] due to their better generalization performance than Adam; and Adam is typically the default for GANs [19], reinforcement learning [21] and transformers [20], mainly due to its better numerical stability and faster convergence than SGD. We aim to validate that ACProp can perform well for both cases.

Image classification with CNN We first conducted experiments on CIFAR10 image classification task with a VGG-11 [31], ResNet34 [6] and DenseNet-121 [32]. We performed extensive hyper-parameter tuning in order to better compare the performance of different optimizers: for SGD we set the momentum as 0.9 which is the default for many cases [6, 32], and search the learning rate between 0.1 and 10^{-5} in the log-grid; for other adaptive optimizers, including AdaBelief, Adam, RAdam, AdamW and AdaShift, we search the learning rate between 0.01 and 10^{-5} in the log-grid, and search ϵ between 10^{-5} and 10^{-10} in the log-grid. We use a weight decay of $5e-2$ for AdamW, and use $5e-4$ for other optimizers. We report the *mean ± std* for the best of each optimizer in Fig. 7: for VGG and ResNet, ACProp achieves comparable results with AdaBelief and outperforms other optimizers; for DenseNet, ACProp achieves the highest accuracy and even outperforms AdaBelief by 0.5%. As in Table 2, for ResNet18 on ImageNet, ACProp outperforms other methods and achieves comparable accuracy to the best of SGD in the literature, validating its generalization performance.

To evaluate the robustness to hyper-parameters, we test the performance of various optimizers under different hyper-parameters with VGG network. We plot the results for ACProp and AdaShift as an example in Fig. 8 and find that ACProp is more robust to hyper-parameters and typically achieves higher accuracy than AdaShift.

Reinforcement learning with DQN We evaluated different optimizers on reinforcement learning with a deep Q-network (DQN) [21] on the four-rooms task [33]. We tune the hyper-parameters in the same setting as previous section. We report the mean and standard deviation of reward (higher is

Table 3: BLEU score (higher is better) on machine translation with Transformer

	Adam	RAdam	AdaShift	AdaBelief	ACProp
DE-EN	34.66±0.014	34.76±0.003	30.18±0.020	35.17±0.015	35.35±0.012
EN-VI	21.83±0.015	22.54±0.005	20.18±0.231	22.45±0.003	22.62±0.008
JA-EN	33.33±0.008	32.23±0.015	25.24±0.151	34.38±0.009	33.70±0.021
RO-EN	29.78±0.003	30.26±0.011	27.86±0.024	30.03±0.012	30.27±0.007

Table 4: FID (lower is better) for GANs

	Adam	RAdam	AdaShift	AdaBelief	ACProp
DCGAN	49.29±0.25	48.24±1.38	99.32±3.82	47.25±0.79	43.43±4.38
RLGAN	38.18±0.01	40.61±0.01	56.18±0.23	36.58±0.12	37.15±0.13
SNGAN	13.14±0.10	13.00±0.04	26.62±0.21	12.70±0.17	12.44±0.02
SAGAN	13.98±0.02	14.25±0.01	22.11±0.25	14.17±0.14	13.54±0.15

Table 5: Performance comparison between AVAGrad and ACProp. \uparrow (\downarrow) represents metrics that upper (lower) is better. * are reported in the AVAGrad paper [28]

	WideResNet Test Error (\downarrow)		Transformer BLEU (\uparrow)		GAN FID (\downarrow)	
	CIFAR10	CIFAR100	DE-EN	RO-EN	DCGAN	SNGAN
AVAGrad	3.80*±0.02	18.76*±0.20	30.23±0.024	27.73±0.134	59.32±3.28	21.02±0.14
ACProp	3.67±0.04	18.72±0.01	35.35±0.012	30.27±0.007	43.34±4.38	12.44±0.02

better) across 10 runs in Fig. 9. ACProp achieves the highest mean reward, validating its numerical stability and good generalization.

Neural machine translation with Transformer We evaluated the performance of ACProp on neural machine translation tasks with a transformer model [20]. For all optimizers, we set learning rate as 0.0002, and search for $\beta_1 \in \{0.9, 0.99, 0.999\}$, $\beta_2 \in \{0.98, 0.99, 0.999\}$ and $\epsilon \in \{10^{-5}, 10^{-6}, \dots, 10^{-16}\}$. As shown in Table. 3, ACProp achieves the highest BLEU score in 3 out of 4 tasks, and consistently outperforms a well-tuned Adam.

Generative Adversarial Networks (GAN) The training of GANs easily suffers from mode collapse and numerical instability [34], hence is a good test for the stability of optimizers. We conducted experiments with Deep Convolutional GAN (DCGAN) [35], Spectral-Norm GAN (SNGAN) [36], Self-Attention GAN (SAGAN) [37] and Relativistic-GAN (RLGAN) [38]. We set $\beta_1 = 0.5$, and search for β_2 and ϵ with the same schedule as previous section. We report the FID [39] on CIFAR10 dataset in Table. 4, where a lower FID represents better quality of generated images. ACProp achieves the best overall FID score and outperforms well-tuned Adam.

Remark Besides AdaShift, we found another async-optimizer named AVAGrad in [28]. Unlike other adaptive optimizers, AVAGrad is not scale-invariant hence the default hyper-parameters are very different from Adam-type ($lr = 0.1, \epsilon = 0.1$). We searched for hyper-parameters for AVAGrad for a much larger range, with ϵ between 1e-8 and 100 in the log-grid, and lr between 1e-6 and 100 in the log-grid. For experiments with a WideResNet, we replace the optimizer in the official implementation for AVAGrad by ACProp, and cite results in the AVAGrad paper. As in Table 5, ACProp consistently outperforms AVAGrad in CNN, Transformer, and GAN training.

6 Related Works

Besides the aforementioned, other variants of Adam include NosAdam [40], Sadam [41], Adax [42]), AdaBound [15] and Yogi [43]. ACProp could be combined with other techniques such as SWATS [44], LookAhead [45] and norm regularization similar to AdamP [46]. Regarding the theoretical analysis, recent research has provided more fine-grained frameworks [47, 48]. Besides first-order methods, recent research approximate second-order methods in deep learning [49, 50, 51].

7 Conclusion

We propose ACProp, a novel first-order gradient optimizer which combines the asynchronous update and centering of second momentum. We demonstrate that ACProp has good theoretical properties: ACProp has a ‘‘always-convergence’’ property for the counter example by Reddi et al. (2018), while sync-optimizers (Adam, RMSProp) could diverge with uncarefully chosen hyper-parameter; for problems with sparse gradient, async-centering (ACProp) has a weaker convergence condition than

async-uncentering (AdaShift); ACProp achieves the optimal convergence rate $O(1/\sqrt{T})$, outperforming the $O(\log T/\sqrt{T})$ rate of RMSProp (Adam), and achieves a tighter upper bound on risk than AdaShift. In experiments, we validate that ACProp has good empirical performance: it achieves good generalization like SGD, fast convergence and training stability like Adam, and often outperforms Adam and AdaBelief.

Acknowledgments and Disclosure of Funding

This research is supported by NIH grant R01NS035193.

References

- [1] Ruoyu Sun, “Optimization for deep learning: theory and algorithms,” *arXiv preprint arXiv:1912.08957*, 2019.
- [2] Herbert Robbins and Sutton Monro, “A stochastic approximation method,” *The annals of mathematical statistics*, pp. 400–407, 1951.
- [3] Yu Nesterov, “A method of solving a convex programming problem with convergence rate $o(1/k^2)$,” in *Sov. Math. Dokl.*, 1983.
- [4] Ilya Sutskever, James Martens, George Dahl, and Geoffrey Hinton, “On the importance of initialization and momentum in deep learning,” in *International conference on machine learning*, 2013, pp. 1139–1147.
- [5] Boris T Polyak, “Some methods of speeding up the convergence of iteration methods,” *USSR Computational Mathematics and Mathematical Physics*, vol. 4, no. 5, pp. 1–17, 1964.
- [6] Kaiming He, Xiangyu Zhang, Shaoqing Ren, and Jian Sun, “Deep residual learning for image recognition,” in *Proceedings of the IEEE conference on computer vision and pattern recognition*, 2016, pp. 770–778.
- [7] Shaoqing Ren, Kaiming He, Ross Girshick, and Jian Sun, “Faster r-cnn: Towards real-time object detection with region proposal networks,” *arXiv preprint arXiv:1506.01497*, 2015.
- [8] Vijay Badrinarayanan, Alex Kendall, and Roberto Cipolla, “Segnet: A deep convolutional encoder-decoder architecture for image segmentation,” *IEEE transactions on pattern analysis and machine intelligence*, vol. 39, no. 12, pp. 2481–2495, 2017.
- [9] John Duchi, Elad Hazan, and Yoram Singer, “Adaptive subgradient methods for online learning and stochastic optimization,” *Journal of machine learning research*, vol. 12, no. Jul, pp. 2121–2159, 2011.
- [10] Matthew D Zeiler, “Adadelta: an adaptive learning rate method,” *arXiv preprint arXiv:1212.5701*, 2012.
- [11] Alex Graves, “Generating sequences with recurrent neural networks,” *arXiv preprint arXiv:1308.0850*, 2013.
- [12] Diederik P Kingma and Jimmy Ba, “Adam: A method for stochastic optimization,” *arXiv preprint arXiv:1412.6980*, 2014.
- [13] Ilya Loshchilov and Frank Hutter, “Decoupled weight decay regularization,” *arXiv preprint arXiv:1711.05101*, 2017.
- [14] Sashank J Reddi, Satyen Kale, and Sanjiv Kumar, “On the convergence of adam and beyond,” *International Conference on Learning Representations*, 2018.
- [15] Liangchen Luo, Yuanhao Xiong, Yan Liu, and Xu Sun, “Adaptive gradient methods with dynamic bound of learning rate,” *arXiv preprint arXiv:1902.09843*, 2019.
- [16] Zhiming Zhou, Qingru Zhang, Guansong Lu, Hongwei Wang, Weinan Zhang, and Yong Yu, “Adashift: Decorrelation and convergence of adaptive learning rate methods,” in *International Conference on Learning Representations*, 2019.
- [17] Liyuan Liu, Haoming Jiang, Pengcheng He, Weizhu Chen, Xiaodong Liu, Jianfeng Gao, and Jiawei Han, “On the variance of the adaptive learning rate and beyond,” *arXiv preprint arXiv:1908.03265*, 2019.

- [18] Juntang Zhuang, Tommy Tang, Sekhar Tatikonda, Nicha Dvornek, Yifan Ding, Xenophon Papademetris, and James S Duncan, “Adabelief optimizer: Adapting stepsizes by the belief in observed gradients,” *arXiv preprint arXiv:2010.07468*, 2020.
- [19] Ian Goodfellow, Jean Pouget-Abadie, Mehdi Mirza, Bing Xu, David Warde-Farley, Sherjil Ozair, Aaron Courville, and Yoshua Bengio, “Generative adversarial nets,” in *Advances in neural information processing systems*, 2014, pp. 2672–2680.
- [20] Ashish Vaswani, Noam Shazeer, Niki Parmar, Jakob Uszkoreit, Llion Jones, Aidan N Gomez, Łukasz Kaiser, and Illia Polosukhin, “Attention is all you need,” *Advances in neural information processing systems*, vol. 30, pp. 5998–6008, 2017.
- [21] Volodymyr Mnih, Koray Kavukcuoglu, David Silver, Alex Graves, Ioannis Antonoglou, Daan Wierstra, and Martin Riedmiller, “Playing atari with deep reinforcement learning,” *arXiv preprint arXiv:1312.5602*, 2013.
- [22] Yasutoshi Ida, Yasuhiro Fujiwara, and Sotetsu Iwamura, “Adaptive learning rate via covariance matrix based preconditioning for deep neural networks,” *arXiv preprint arXiv:1605.09593*, 2016.
- [23] Yossi Arjevani, Yair Carmon, John C Duchi, Dylan J Foster, Nathan Srebro, and Blake Woodworth, “Lower bounds for non-convex stochastic optimization,” *arXiv preprint arXiv:1912.02365*, 2019.
- [24] Geoffrey Hinton, “Rmsprop: Divide the gradient by a running average of its recent magnitude,” *Coursera*, 2012.
- [25] Naichen Shi, Dawei Li, Mingyi Hong, and Ruoyu Sun, “{RMS}prop can converge with proper hyper-parameter,” in *International Conference on Learning Representations*, 2021.
- [26] Xiangyi Chen, Sijia Liu, Ruoyu Sun, and Mingyi Hong, “On the convergence of a class of adam-type algorithms for non-convex optimization,” *arXiv preprint arXiv:1808.02941*, 2018.
- [27] Fangyu Zou, Li Shen, Zequn Jie, Weizhong Zhang, and Wei Liu, “A sufficient condition for convergences of adam and rmsprop,” in *Proceedings of the IEEE/CVF Conference on Computer Vision and Pattern Recognition*, 2019, pp. 11127–11135.
- [28] Pedro Savarese, David McAllester, Sudarshan Babu, and Michael Maire, “Domain-independent dominance of adaptive methods,” *arXiv preprint arXiv:1912.01823*, 2019.
- [29] Xiaoyu Li and Francesco Orabona, “On the convergence of stochastic gradient descent with adaptive stepsizes,” in *The 22nd International Conference on Artificial Intelligence and Statistics*. PMLR, 2019, pp. 983–992.
- [30] Jinghui Chen and Quanquan Gu, “Closing the generalization gap of adaptive gradient methods in training deep neural networks,” *arXiv preprint arXiv:1806.06763*, 2018.
- [31] Karen Simonyan and Andrew Zisserman, “Very deep convolutional networks for large-scale image recognition,” *arXiv preprint arXiv:1409.1556*, 2014.
- [32] Gao Huang, Zhuang Liu, Laurens Van Der Maaten, and Kilian Q Weinberger, “Densely connected convolutional networks,” in *Proceedings of the IEEE conference on computer vision and pattern recognition*, 2017, pp. 4700–4708.
- [33] Richard S Sutton, Doina Precup, and Satinder Singh, “Between mdps and semi-mdps: A framework for temporal abstraction in reinforcement learning,” *Artificial intelligence*, vol. 112, no. 1-2, pp. 181–211, 1999.
- [34] Tim Salimans, Ian Goodfellow, Wojciech Zaremba, Vicki Cheung, Alec Radford, and Xi Chen, “Improved techniques for training gans,” in *Advances in neural information processing systems*, 2016, pp. 2234–2242.
- [35] Alec Radford, Luke Metz, and Soumith Chintala, “Unsupervised representation learning with deep convolutional generative adversarial networks,” *arXiv preprint arXiv:1511.06434*, 2015.
- [36] Takeru Miyato, Toshiki Kataoka, Masanori Koyama, and Yuichi Yoshida, “Spectral normalization for generative adversarial networks,” *arXiv preprint arXiv:1802.05957*, 2018.
- [37] Han Zhang, Ian Goodfellow, Dimitris Metaxas, and Augustus Odena, “Self-attention generative adversarial networks,” in *International conference on machine learning*. PMLR, 2019, pp. 7354–7363.

- [38] Alexia Jolicoeur-Martineau, “The relativistic discriminator: a key element missing from standard gan,” *arXiv preprint arXiv:1807.00734*, 2018.
- [39] Martin Heusel, Hubert Ramsauer, Thomas Unterthiner, Bernhard Nessler, and Sepp Hochreiter, “Gans trained by a two time-scale update rule converge to a local nash equilibrium,” in *Advances in neural information processing systems*, 2017, pp. 6626–6637.
- [40] Haiwen Huang, Chang Wang, and Bin Dong, “Nostalgic adam: Weighting more of the past gradients when designing the adaptive learning rate,” *arXiv preprint arXiv:1805.07557*, 2018.
- [41] Guanghui Wang, Shiyin Lu, Weiwei Tu, and Lijun Zhang, “Sadam: A variant of adam for strongly convex functions,” *arXiv preprint arXiv:1905.02957*, 2019.
- [42] Wenjie Li, Zhaoyang Zhang, Xinjiang Wang, and Ping Luo, “Adax: Adaptive gradient descent with exponential long term memory,” *arXiv preprint arXiv:2004.09740*, 2020.
- [43] Manzil Zaheer, Sashank Reddi, Devendra Sachan, Satyen Kale, and Sanjiv Kumar, “Adaptive methods for nonconvex optimization,” in *Advances in neural information processing systems*, 2018, pp. 9793–9803.
- [44] Pavel Izmailov, Dmitrii Podoprikin, Timur Garipov, Dmitry Vetrov, and Andrew Gordon Wilson, “Averaging weights leads to wider optima and better generalization,” *arXiv preprint arXiv:1803.05407*, 2018.
- [45] Michael Zhang, James Lucas, Jimmy Ba, and Geoffrey E Hinton, “Lookahead optimizer: k steps forward, 1 step back,” in *Advances in Neural Information Processing Systems*, 2019, pp. 9593–9604.
- [46] Byeongho Heo, Sanghyuk Chun, Seong Joon Oh, Dongyoon Han, Sangdoon Yun, Gyuwan Kim, Youngjung Uh, and Jung-Woo Ha, “Adamp: Slowing down the slowdown for momentum optimizers on scale-invariant weights,” in *Proceedings of the International Conference on Learning Representations (ICLR), Online*, 2021, pp. 3–7.
- [47] Ahmet Alacaoglu, Yura Malitsky, Panayotis Mertikopoulos, and Volkan Cevher, “A new regret analysis for adam-type algorithms,” in *International Conference on Machine Learning*. PMLR, 2020, pp. 202–210.
- [48] Xiaoyu Li, Zhenxun Zhuang, and Francesco Orabona, “Exponential step sizes for non-convex optimization,” *arXiv preprint arXiv:2002.05273*, 2020.
- [49] James Martens, “Deep learning via hessian-free optimization.,” in *ICML*, 2010, vol. 27, pp. 735–742.
- [50] Zhewei Yao, Amir Gholami, Sheng Shen, Kurt Keutzer, and Michael W Mahoney, “Adahessian: An adaptive second order optimizer for machine learning,” *arXiv preprint arXiv:2006.00719*, 2020.
- [51] Xuezhe Ma, “Apollo: An adaptive parameter-wise diagonal quasi-newton method for nonconvex stochastic optimization,” *arXiv preprint arXiv:2009.13586*, 2020.
- [52] Shi Naichen, Li Dawei, Hong Mingyi, and Sun Ruoyu, “Rmsprop can converge with proper hyper-parameter,” *ICLR*, 2021.

Contents

1	Introduction	1
2	Overview of algorithms	2
2.1	Notations	2
2.2	Algorithms	2
3	Analyze the conditions for convergence	3
3.1	<i>Sync vs Async</i>	3
3.2	<i>Async-Uncenter vs Async-Center</i>	5

4	Analysis on convergence rate	6
5	Experiments	8
6	Related Works	9
7	Conclusion	9
A	Analysis on convergence conditions	14
A.1	Convergence analysis for Problem 1 in the main paper	14
A.1.1	Numerical validations	17
A.2	Convergence analysis for Problem 2 in the main paper	18
A.3	Numerical experiments	20
B	Convergence Analysis for stochastic non-convex optimization	23
B.1	Problem definition and assumptions	23
B.2	Convergence analysis of Async-optimizers in stochastic non-convex optimization .	23
B.2.1	Validation on numerical accuracy of sum of generalized harmonic series . .	25
B.3	Convergence analysis of Async-moment-optimizers in stochastic non-convex optimization	25
C	Experiments	28
C.1	Centering of second momentum does not suffer from numerical issues	28
C.2	Image classification with CNN	29
C.3	Neural Machine Translation with Transformers	31
C.4	Generative adversarial networks	32

A Analysis on convergence conditions

A.1 Convergence analysis for Problem 1 in the main paper

Lemma A.1. *There exists an online convex optimization problem where Adam (and RMSprop) has non-zero average regret, and one of the problem is in the form*

$$f_t(x) = \begin{cases} Px, & \text{if } t \bmod P = 1 \\ -x, & \text{Otherwise} \end{cases} \quad x \in [-1, 1], \exists P \in \mathbb{N}, P \geq 3 \quad (8)$$

Proof. See [14] Thm.1 for proof. \square

Lemma A.2. *For the problem defined above, there's a threshold of β_2 above which RMSprop converge.*

Proof. See [52] for details. \square

Lemma A.3 (Lemma.3.3 in the main paper). *For the problem defined by Eq. (8), ACProp algorithm converges $\forall \beta_1, \beta_2 \in (0, 1), \forall P \in \mathbb{N}, P \geq 3$.*

Proof. We analyze the limit behavior of ACProp algorithm. Since the observed gradient is periodic with an integer period P , we analyze one period from with indices from kP to $kP + P$, where k is an integer going to $+\infty$.

From the update of ACProp, we observe that:

$$m_{kP} = (1 - \beta_1) \sum_{i=1}^{kP} \beta_1^{kP-i} \times (-1) + (1 - \beta_1) \sum_{j=0}^{k-1} \beta_1^{kP-(jP+1)} (P+1) \quad (9)$$

(For each observation with gradient P , we break it into $P = -1 + (P+1)$)

$$= -(1 - \beta_1) \sum_{i=1}^{kP} \beta_1^{kP-i} + (1 - \beta_1)(P+1)\beta_1^{-1} \sum_{j=0}^{k-1} \beta_1^{P(k-j)} \quad (10)$$

$$= -(1 - \beta_1^{kP}) + (1 - \beta_1)(P+1)\beta_1^{P-1} \frac{1 - \beta_1^{(k-1)P}}{1 - \beta_1^P} \quad (11)$$

$$\lim_{k \rightarrow \infty} m_{kP} = -1 + (P+1)(1 - \beta_1)\beta_1^{P-1} \frac{1}{1 - \beta_1^P} = \frac{(P+1)\beta_1^{P-1} - P\beta_1^P - 1}{1 - \beta_1^P} \quad (12)$$

(Since $\beta_1 \in [0, 1)$)

Next, we derive $\lim_{k \rightarrow \infty} S_{kP}$. Note that the observed gradient is periodic, and $\lim_{k \rightarrow \infty} m_{kP} = \lim_{k \rightarrow \infty} m_{kP+P}$, hence $\lim_{k \rightarrow \infty} S_{kP} = \lim_{k \rightarrow \infty} S_{kP+P}$. Start from index kP , we derive variables up to $kP + P$ with ACProp algorithm.

$$\begin{aligned} \text{index} &= kP, \\ m_{kP}, S_{kP} \end{aligned} \quad (13)$$

$$\begin{aligned} \text{index} &= kP + 1, \\ m_{kP+1} &= \beta_1 m_0 + (1 - \beta_1)P \end{aligned} \quad (14)$$

$$S_{kP+1} = \beta_2 S_{kP} + (1 - \beta_2)(P - m_{kP})^2 \quad (15)$$

$$\begin{aligned} \text{index} &= kP + 2, \\ m_{kP+2} &= \beta_1 m_{kP+1} + (1 - \beta_1) \times (-1) \end{aligned} \quad (16)$$

$$= \beta_1^2 m_{kP} + (1 - \beta_1)\beta_1 P + (1 - \beta_1) \times (-1) \quad (17)$$

$$S_{kP+2} = \beta_2 S_{kP+1} + (1 - \beta_2)(-1 - m_{kP+1})^2 \quad (18)$$

$$= \beta_2^2 S_{kP} + (1 - \beta_2)\beta_2(P - m_{kP})^2 + (1 - \beta_2)[\beta_1(P - m_{kP}) - (P+1)]^2 \quad (19)$$

$$index = kP + 3,$$

$$m_{kP+3} = \beta_1 m_{kP+2} + (1 - \beta_1) \times (-1) \quad (20)$$

$$= \beta_1^3 m_{kP} + (1 - \beta_1) \beta_1^2 P + (1 - \beta_1) \beta_1 \times (-1) + (1 - \beta_1) \times (-1) \quad (21)$$

$$S_{kP+3} = \beta_2 S_2 + (1 - \beta_2) (-1 - m_{kP+2})^2 \quad (22)$$

$$\begin{aligned} &= \beta_2^3 S_{kP} + (1 - \beta_2) \beta_2^2 (P - m_{kP})^2 \\ &+ (1 - \beta_2) \beta_2 [\beta_1 (P - m_{kP}) - (P + 1)]^2 (\beta_2 + \beta_1^2) \end{aligned} \quad (23)$$

$$index = kP + 4,$$

$$m_{kP+4} = \beta_1^4 m_{kP} + (1 - \beta_1) \beta_1^3 P + (-1)(1 - \beta_1)(\beta_1^2 + \beta_1 + 1) \quad (24)$$

$$S_{kP+4} = \beta_2 S_{kP+3} + (1 - \beta_2) (-1 - m_{kP+3})^2 \quad (25)$$

$$\begin{aligned} &= \beta_2^4 S_{kP} + (1 - \beta_2) \beta_2^3 (P - m_{kP})^2 \\ &+ (1 - \beta_2) \beta_2 [\beta_1 (P - m_{kP}) - (P + 1)]^2 (\beta_2^2 + \beta_2 \beta_1^2 + \beta_1^4) \end{aligned} \quad (26)$$

...

$$index = kP + P,$$

$$m_{kP+P} = \beta_1^P m_{kP} + (1 - \beta_1) \beta_1^{P-1} P + (-1)(1 - \beta_1) [\beta_1^{P-2} + \beta_1^{P-3} + \dots + 1] \quad (27)$$

$$= \beta_1^P m_{kP} + (1 - \beta_1) \beta_1^{P-1} P + (\beta_1 - 1) \frac{1 - \beta_1^{P-1}}{1 - \beta_1} \quad (28)$$

$$\begin{aligned} S_{kP+P} &= \beta_2^P S_{kP} + (1 - \beta_2) \beta_2^{P-1} (P - m_{kP})^2 \\ &+ (1 - \beta_2) [\beta_1 (P - m_{kP}) - (P + 1)]^2 (\beta_2^{P-2} + \beta_2^{P-3} \beta_1^2 + \dots + \beta_2^0 \beta_1^{2P-4}) \end{aligned} \quad (29)$$

$$\begin{aligned} &= \beta_2^P S_{kP} + (1 - \beta_2) \beta_2^{P-1} (P - m_{kP})^2 \\ &+ (1 - \beta_2) [\beta_1 (P - m_{kP}) - (P + 1)]^2 \beta_2^{P-2} \frac{1 - (\beta_1^2/\beta_2)^{P-1}}{1 - (\beta_1^2/\beta_2)} \end{aligned} \quad (30)$$

As k goes to $+\infty$, we have

$$\lim_{k \rightarrow \infty} m_{kP+P} = \lim_{k \rightarrow \infty} m_{kP} \quad (31)$$

$$\lim_{k \rightarrow \infty} S_{kP+P} = \lim_{k \rightarrow \infty} S_{kP} \quad (32)$$

From Eq. (28) we have:

$$m_{kP+P} = \frac{(P + 1) \beta_1^{P-1} - P \beta_1^P - 1}{1 - \beta_1^P} \quad (33)$$

which matches our result in Eq. (13). Similarly, from Eq. (30), take limit of $k \rightarrow \infty$, and combine with Eq. (32), we have

$$\lim_{k \rightarrow \infty} S_{kP} = \frac{1 - \beta_2}{1 - \beta_2^P} \left[\beta_2^{P-1} (P - \lim_{k \rightarrow \infty} m_{kP})^2 + [\beta_1 (P - \lim_{k \rightarrow \infty} m_{kP}) - (P + 1)]^2 \beta_2^{P-2} \frac{1 - (\beta_1^2/\beta_2)^{P-1}}{1 - (\beta_1^2/\beta_2)} \right] \quad (34)$$

Since we have the exact expression for the limit, it's trivial to check that

$$S_i \geq S_{kP}, \quad \forall i \in [kP + 1, kP + P], i \in \mathbb{N}, k \rightarrow \infty \quad (35)$$

Intuitively, suppose for some time period, we only observe a constant gradient -1 without observing the outlier gradient (P); the longer the length of this period, the smaller is the corresponding S value, because S records the difference between observations. Note that since last time that outlier gradient (P) is observed (at index $kP + 1 - P$), index kP has the longest distance from index $kP + 1 - P$ without observing the outlier gradient (P). Therefore, S_{kP} has the smallest value within a period of P as k goes to infinity.

For step $kP + 1$ to $kP + P$, the update on parameter is:

$$index = kP + 1, -\Delta_x^{kP+1} = \frac{\alpha_0}{\sqrt{kP + 1}} \frac{P}{\sqrt{S_{kP}} + \epsilon} \quad (36)$$

$$index = kP + 2, -\Delta_x^{kP+2} = \frac{\alpha_0}{\sqrt{kP+2}} \frac{-1}{\sqrt{S_{kP+1} + \epsilon}} \quad (37)$$

...

$$index = kP + P, -\Delta_x^{kP+P} = \frac{\alpha_0}{\sqrt{kP+P}} \frac{-1}{\sqrt{S_{kP+P-1} + \epsilon}} \quad (38)$$

So the negative total update within this period is:

$$\frac{\alpha_0}{\sqrt{kP+1}} \frac{P}{\sqrt{S_{kP} + \epsilon}} - \underbrace{\left[\frac{\alpha_0}{\sqrt{kP+2}} \frac{1}{\sqrt{S_{kP+1} + \epsilon}} + \dots + \frac{\alpha_0}{\sqrt{kP+P}} \frac{1}{\sqrt{S_{kP+P-1} + \epsilon}} \right]}_{P-1 \text{ terms}} \quad (39)$$

$$\geq \frac{\alpha_0}{\sqrt{kP+1}} \frac{P}{\sqrt{S_{kP} + \epsilon}} - \underbrace{\left[\frac{\alpha_0}{\sqrt{kP+1}} \frac{1}{\sqrt{S_{kP} + \epsilon}} + \dots + \frac{\alpha_0}{\sqrt{kP+1}} \frac{1}{\sqrt{S_{kP} + \epsilon}} \right]}_{P-1 \text{ terms}} \quad (40)$$

(Since S_{kP} is the minimum within the period)

$$= \frac{\alpha_0}{\sqrt{S_{kP} + \epsilon}} \frac{1}{\sqrt{kP+1}} \quad (41)$$

where α_0 is the initial learning rate. Note that the above result hold for every period of length P as k gets larger. Therefore, for some K such that for every $k > K$, m_{kP} and S_{kP} are close enough to their limits, the total update after K is:

$$\sum_{k=K}^{\infty} \frac{\alpha_0}{\sqrt{S_{kP} + \epsilon}} \frac{1}{\sqrt{kP+1}} \approx \frac{\alpha_0}{\sqrt{\lim_{k \rightarrow \infty} S_{kP} + \epsilon}} \frac{1}{\sqrt{P}} \sum_{k=K}^{\infty} \frac{1}{\sqrt{k}} \text{ If } K \text{ is sufficiently large} \quad (42)$$

where $\lim_{k \rightarrow \infty} S_{kP}$ is a constant determined by Eq. (34). Note that this is the negative update; hence ACProp goes to the negative direction, which is what we expected for this problem. Also considering that $\sum_{k=K}^{\infty} \frac{1}{\sqrt{k}} \rightarrow \infty$, hence ACProp can go arbitrarily far in the correct direction if the algorithm runs for infinitely long, therefore the bias caused by first K steps will vanish with running time. Furthermore, since x lies in the bounded region of $[-1, 1]$, if the updated result falls out of this region, it can always be clipped. Therefore, for this problem, ACProp always converge to $x = -1, \forall \beta_1, \beta_2 \in (0, 1)$. When $\beta_2 = 1$, the denominator won't update, and ACProp reduces to SGD (with momentum), and it's shown to converge. \square

Lemma A.4. For any constant $\beta_1, \beta_2 \in [0, 1)$ such that $\beta_1 < \sqrt{\beta_2}$, there is a stochastic convex optimization problem for which Adam does not converge to the optimal solution. One example of such stochastic problem is:

$$f_t(x) = \begin{cases} Px & \text{with probability } \frac{1+\delta}{P+1} \\ -x & \text{with probability } \frac{P-\delta}{P+1} \end{cases} \quad x \in [-1, 1] \quad (43)$$

Proof. See Thm.3 in [14]. \square

Lemma A.5. For the stochastic problem defined by Eq. (43), ACProp converge to the optimal solution, $\forall \beta_1, \beta_2 \in (0, 1)$.

Proof. The update at step t is:

$$\Delta_x^t = -\frac{\alpha_0}{\sqrt{t}} \frac{g_t}{\sqrt{S_{t-1} + \epsilon}} \quad (44)$$

Take expectation conditioned on observations up to step $t-1$, we have:

$$\mathbb{E} \Delta_x^t = -\frac{\alpha_0}{\sqrt{t}} \frac{\mathbb{E}_t g_t}{\sqrt{S_{t-1} + \epsilon}} \quad (45)$$

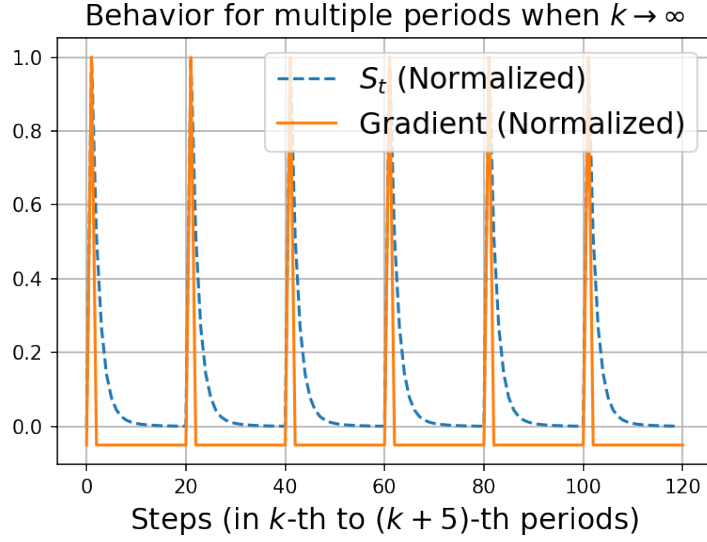


Figure 10: Behavior of S_t and g_t in ACProp of multiple periods for problem (1). Note that as $k \rightarrow \infty$, the behavior of ACProp is periodic.

$$= -\frac{\alpha_0}{\sqrt{t}(\sqrt{S_{t-1}} + \epsilon)} \mathbb{E}_t g_t \quad (46)$$

$$= -\frac{\alpha_0}{\sqrt{t}(\sqrt{S_{t-1}} + \epsilon)} \left[P \frac{1 + \delta}{P + 1} - \frac{P - \delta}{P + 1} \right] \quad (47)$$

$$= -\frac{\alpha_0 \delta}{\sqrt{t}(\sqrt{S_{t-1}} + \epsilon)} \quad (48)$$

$$\leq -\frac{\alpha_0 \delta}{\sqrt{t}(P + 1 + \epsilon)} \quad (49)$$

where the last inequality is due to $S_t \leq (P + 1)^2$, because S_t is a smoothed version of squared difference between gradients, and the maximum difference in gradient is $P + 1$. Therefore, for every step, ACProp is expected to move in the negative direction, also considering that $\sum_{t=1}^{\infty} \frac{1}{\sqrt{t}} \rightarrow \infty$, and whenever $x < -1$ we can always clip it to -1 , hence ACProp will drift x to -1 , which is the optimal value. \square

A.1.1 Numerical validations

We validate our analysis above in numerical experiments, and plot the curve of S_t and g_t for multiple periods (as $k \rightarrow \infty$) in Fig. 10 and zoom in to a single period in Fig. 11. Note that the largest gradient P (normalized as 1) appears at step $kP + 1$, and S takes it minimal at step kP (e.g. S_{kP} is the smallest number within a period). Note the update for step $kP + 1$ is $g_{kP+1}/\sqrt{S_{kP}}$, it's the largest gradient divided the smallest denominator, hence the net update within a period pushes x towards the optimal point.

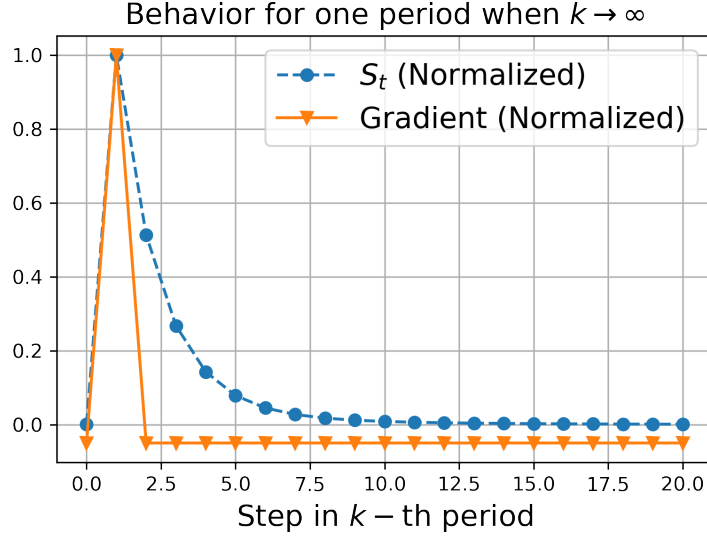


Figure 11: Behavior of S_t and g_t in ACProp of one period for problem (1).

A.2 Convergence analysis for Problem 2 in the main paper

Lemma A.6 (Lemma 3.4 in the main paper). *For the problem defined by Eq. (50), consider the hyper-parameter tuple (β_1, β_2, P) , there exists cases where ACProp converges but AdaShift with $n = 1$ diverges, but not vice versa.*

$$f_t(x) = \begin{cases} P/2 \times x, & t \% P == 1 \\ -x, & t \% P == P - 2 \\ 0, & \text{otherwise} \end{cases} \quad P > 3, P \in \mathbb{N}, x \in [0, 1]. \quad (50)$$

Proof. The proof is similar to Lemma. A.3, we derive the limit behavior of different methods.

$$\text{index} = kP,$$

$$m_{kP}, v_{kP}, s_{kP}$$

$$\text{index} = kP + 1,$$

$$m_{kP+1} = m_{kP}\beta_1 + (1 - \beta_1)P/2 \quad (51)$$

$$v_{kP+1} = v_{kP}\beta_2 + (1 - \beta_2)P^2/4 \quad (52)$$

$$s_{kP+1} = s_{kP}\beta_2 + (1 - \beta_2)(P/2 - m_{kP})^2 \quad (53)$$

...

$$\text{index} = kP + P - 2,$$

$$m_{kP+P-2} = m_{kP}\beta_1^{P-2} + (1 - \beta_1)\frac{P}{2}\beta_1^{P-3} + (1 - \beta_1) \times (-1) \quad (54)$$

$$v_{kP+P-2} = v_{kP}\beta_2^{P-2} + (1 - \beta_2)\frac{P^2}{4}\beta_2^{P-3} + (1 - \beta_2) \quad (55)$$

$$s_{kP+P-2} = s_{kP}\beta_2^{P-2} + (1 - \beta_2)\beta_2^{P-3}\left(\frac{P}{2} - m_{kP}\right)^2 + (1 - \beta_2)\beta_2^{P-4}m_{kP+1}^2 + \dots \\ + (1 - \beta_2)\beta_2 m_{kP+P-4}^2 + (1 - \beta_2)(m_{kP+P-3} + 1)^2 \quad (56)$$

$$\text{index} = kP + P - 1,$$

$$m_{kP+P-1} = m_{kP+P-1}\beta_1 \quad (57)$$

$$v_{kP+P-1} = v_{kP+P-2}\beta_2 \quad (58)$$

$$s_{kP+P-1} = s_{kP}\beta_2^{P-1} + (1 - \beta_2)\beta_2^{P-1}\left(\frac{P}{2} - m_{kP}\right)^2 + (1 - \beta_2)\beta_2^{P-3}m_{kP+1}^2 + \dots$$

$$+ (1 - \beta_2)\beta_2^2 m_{kP+P-4}^2 + (1 - \beta_2)\beta_2(m_{kP+P-3} + 1)^2 + (1 - \beta_2)m_{kP+P-2}^2 \quad (59)$$

index = $kP + P$,

$$m_{kP+P} = m_{kP}\beta_1^P + (1 - \beta_1)\frac{P}{2}\beta_1^{P-1} + (1 - \beta_1)(-1)\beta_1^2 \quad (60)$$

$$v_{kP+P} = v_{kP}\beta_2^P + (1 - \beta_2)\frac{P^2}{4}\beta_2^{P-1} + (1 - \beta_2)\beta_2^2 \quad (61)$$

$$\begin{aligned} s_{kP+P} &= s_{kP}\beta_2^P + (1 - \beta_2)\beta_2^{P-1}\left(\frac{P}{2} - m_{kP}\right)^2 + (1 - \beta_2)\beta_2^{P-2}m_{kP+1}^2 + \dots \\ &+ (1 - \beta_2)\beta_2^3 m_{kP+P-4}^2 + (1 - \beta_2)\beta_2^2(m_{kP+P-3} + 1)^2 \\ &+ (1 - \beta_2)m_{kP+P-2}^2\beta_2 + (1 - \beta_2)m_{kP+P-1}^2 \end{aligned} \quad (62)$$

Next, we derive the exact expression using the fact that the problem is periodic, hence $\lim_{k \rightarrow \infty} m_{kP} = \lim_{k \rightarrow \infty} m_{kP+P}$, $\lim_{k \rightarrow \infty} s_{kP} = \lim_{k \rightarrow \infty} s_{kP+P}$, $\lim_{k \rightarrow \infty} v_{kP} = \lim_{k \rightarrow \infty} v_{kP+P}$, hence we have:

$$\lim_{k \rightarrow \infty} m_{kP} = \lim_{k \rightarrow \infty} m_{kP}\beta_1^P + (1 - \beta_1)\frac{P}{2}\beta_1^{P-1} + (1 - \beta_1)(-1)\beta_1^2 \quad (63)$$

$$\lim_{k \rightarrow \infty} m_{kP} = \frac{1 - \beta_1}{1 - \beta_1^P} \left[\frac{P}{2}\beta_1^{P-1} - \beta_1^2 \right] \quad (64)$$

$$\lim_{k \rightarrow \infty} m_{kP-1} = \frac{1}{\beta_1} \lim_{k \rightarrow \infty} m_{kP} \quad (65)$$

$$\lim_{k \rightarrow \infty} m_{kP-2} = \frac{1}{\beta_1} \left[\lim_{k \rightarrow \infty} m_{kP-1} - (1 - \beta_1)0 \right] \quad (66)$$

$$\lim_{k \rightarrow \infty} m_{kP-3} = \frac{1}{\beta_1} \left[\lim_{k \rightarrow \infty} m_{kP-2} - (1 - \beta_1)(-1) \right] \quad (67)$$

Similarly, we can get

$$\lim_{k \rightarrow \infty} v_{kP} = \frac{1 - \beta_2}{1 - \beta_2^P} \left[\frac{P^2}{4}\beta_2^{P-1} + \beta_2^2 \right] \quad (68)$$

$$\lim_{k \rightarrow \infty} v_{kP-1} = \frac{1}{\beta_2} \lim_{k \rightarrow \infty} v_{kP} \quad (69)$$

$$\lim_{k \rightarrow \infty} v_{kP-2} = \frac{1}{\beta_2} \lim_{k \rightarrow \infty} v_{kP-1} \quad (70)$$

$$\lim_{k \rightarrow \infty} v_{kP-3} = \frac{1}{\beta_2} \left[\lim_{k \rightarrow \infty} v_{kP-2} - (1 - \beta_2) \times 1^2 \right] \quad (71)$$

For ACProp, we have the following results:

$$\begin{aligned} \lim_{k \rightarrow \infty} s_{kP} &= \lim_{k \rightarrow \infty} \frac{1 - \beta_2}{1 - \beta_2^P} \left[\beta_2^{P-4} \left(\frac{P}{2} - m_{kP} \right)^2 + \beta_2^3 \frac{\beta_2^{P-5} - \beta_1^{2(P-4)}\beta_2}{1 - \beta_1^2\beta_2} + \beta_2^2(m_{kP+P-3} + 1)^2 \right. \\ &\left. + \beta_2 m_{kP+P-2}^2 + m_{kP+P-1}^2 \right] \end{aligned} \quad (72)$$

$$\lim_{k \rightarrow \infty} s_{kP-1} = \lim_{k \rightarrow \infty} \frac{1}{\beta_2} \left[s_{kP} - (1 - \beta_2)m_{kP}^2 \right] \quad (73)$$

$$\lim_{k \rightarrow \infty} s_{kP-2} = \lim_{k \rightarrow \infty} \frac{1}{\beta_2} \left[s_{kP-1} - (1 - \beta_2)m_{kP-1}^2 \right] \quad (74)$$

$$\lim_{k \rightarrow \infty} s_{kP-3} = \lim_{k \rightarrow \infty} \frac{1}{\beta_2} \left[s_{kP-2} - (1 - \beta_2)(m_{kP-2} + 1)^2 \right] \quad (75)$$

$$(76)$$

Within each period, ACprop will perform a positive update $P/(2\sqrt{s^+})$ and a negative update $-1/\sqrt{s^-}$, where s^+ (s^-) is the value of denominator before observing positive (negative) gradient. Similar notations for v^+ and v^- in AdaShift, where $s^+ = s_{kP}$, $s^- = s_{kP-3}$, $v^+ = v_{kP}$, $v^- =$

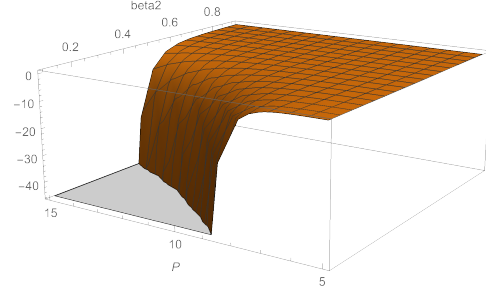
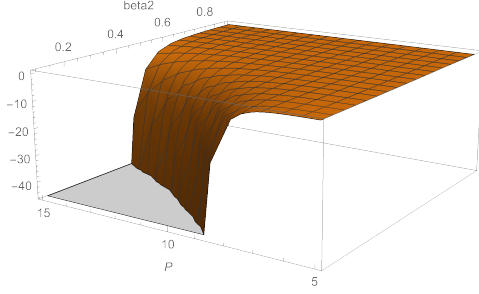


Figure 12: Value of $\frac{s^+}{s^-} - \frac{v^+}{v^-}$ when $\beta_1 = 0.2$ Figure 13: Value of $\frac{s^+}{s^-} - \frac{v^+}{v^-}$ when $\beta_1 = 0.9$

$v_k P - 3$. A net update in the correct direction requires $\frac{P}{2\sqrt{s^+}} > \frac{1}{\sqrt{s^-}}$, (or $s^+/s^- < P^2/4$). Since we have the exact expression for these terms in the limit sense, it's trivial to verify that $s^+/s^- \leq v^+/v^-$ (e.g. the value $\frac{s^+}{s^-} - \frac{v^+}{v^-}$ is negative as in Fig. 12 and 13), hence ACProp is easier to satisfy the convergence condition. \square

A.3 Numerical experiments

We conducted more experiments to validate previous claims. We plot the area of convergence for different β_1 values for problem (1) in Fig. 14 to Fig. 16, and validate the always-convergence property of ACProp with different values of β_1 . We also plot the area of convergence for problem (2) defined by Eq. (50), results are shown in Fig. 17 to Fig. 19. Note that for this problem the always-convergence does not hold, but ACProp has a much larger area of convergence than AdaShift.

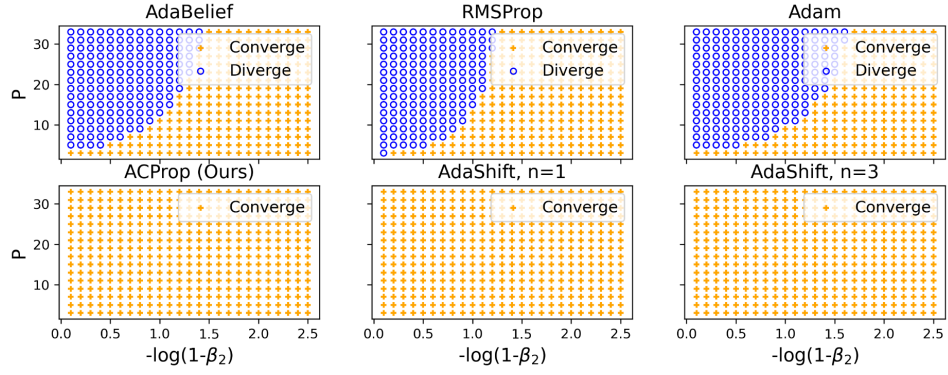


Figure 14: Numerical experiments on problem (1) with $\beta_1 = 0.5$

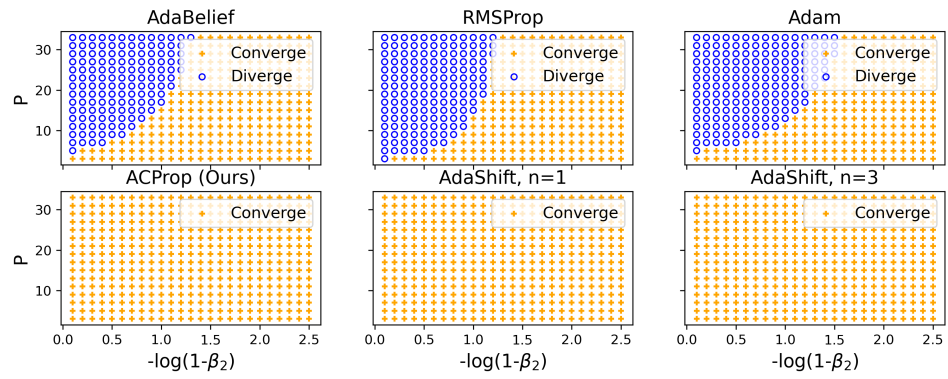


Figure 15: Numerical experiments on problem (1) with $\beta_1 = 0.5$

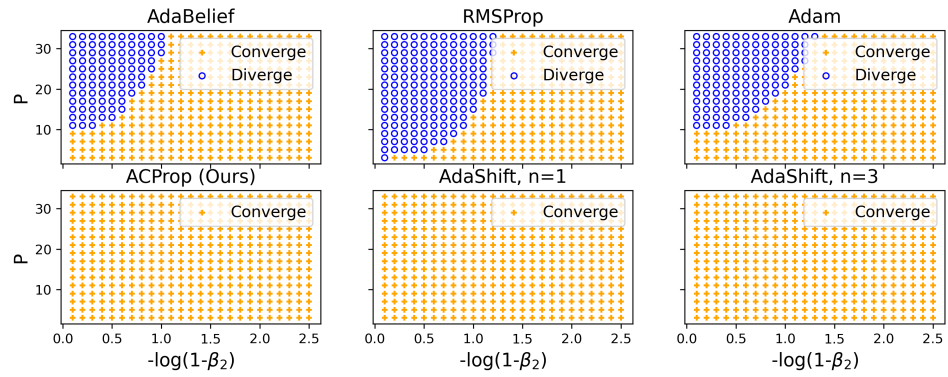


Figure 16: Numerical experiments on problem (1) with $\beta_1 = 0.9$

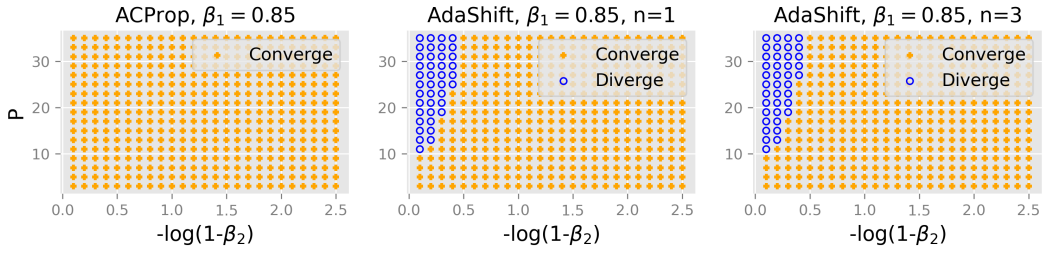


Figure 17: Numerical experiments on problem (43) with $\beta_1 = 0.85$

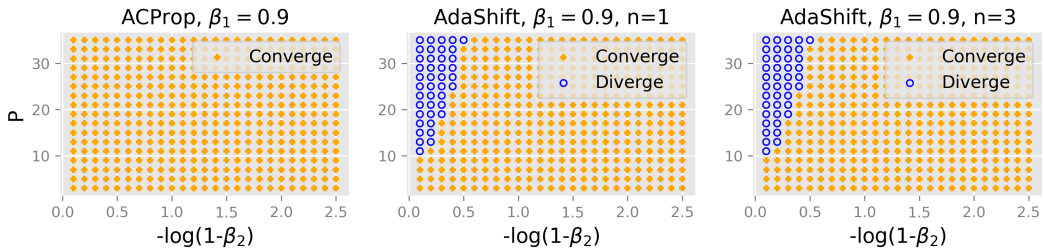


Figure 18: Numerical experiments on problem (43) with $\beta_1 = 0.9$

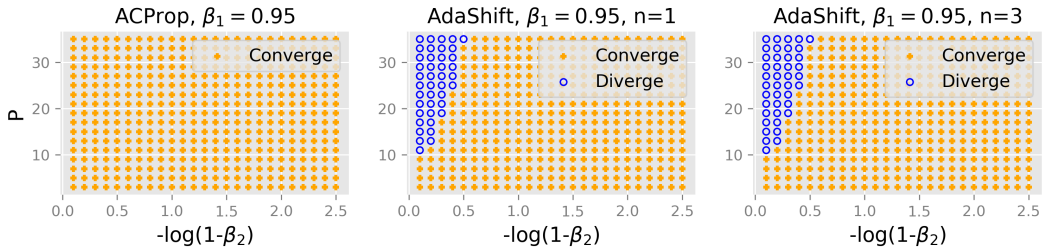
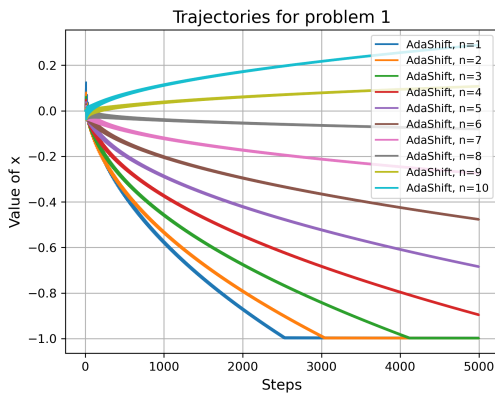
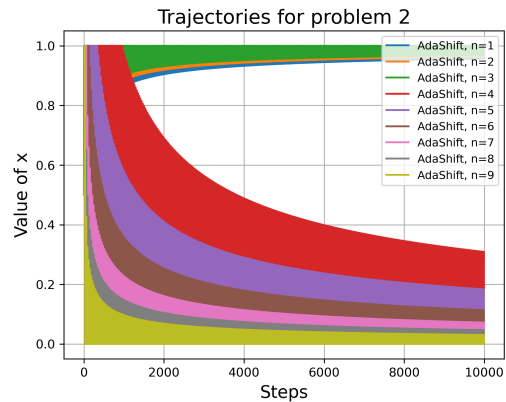


Figure 19: Numerical experiments on problem (43) with $\beta_1 = 0.95$



(a) Trajectories of AdaShift with various n for problem (1). Note that optimal is $x^* = -1$. Note that convergence of problem (1) requires a small delay step n , but convergence of problem (2) requires a large n , hence there's no good criterion to select an optimal n .



(b) Trajectories of AdaShift with various n for problem (43). Note that optimal is $x^* = 0.0$, and the trajectories are oscillating at a high frequency hence appears to be spanning an area.

B Convergence Analysis for stochastic non-convex optimization

B.1 Problem definition and assumptions

The problem is defined as:

$$\min_{x \in \mathbb{R}^d} f(x) = \mathbb{E}[F(x, \xi)] \quad (77)$$

where x typically represents parameters of the model, and ξ represents data which typically follows some distribution.

We mainly consider the stochastic non-convex case, with assumptions below.

A.1 f is continuously differentiable, f is lower-bounded by f^* . $\nabla f(f)$ is globally Lipschitz continuous with constant L :

$$\|\nabla f(x) - \nabla f(y)\| \leq L\|x - y\| \quad (78)$$

A.2 For any iteration t , g_t is an unbiased estimator of $\nabla f(x_t)$ with variance bounded by σ^2 . The norm of g_t is upper-bounded by M_g .

$$(a) \quad \mathbb{E}g_t = \nabla f(x_t) \quad (79)$$

$$(b) \quad \mathbb{E}[\|g_t - \nabla f(x_t)\|^2] \leq \sigma^2 \quad (80)$$

B.2 Convergence analysis of Async-optimizers in stochastic non-convex optimization

Theorem B.1 (Thm.4.1 in the main paper). *Under assumptions A.1-2, assume f is upper bounded by M_f , with learning rate schedule as*

$$\alpha_t = \alpha_0 t^{-\eta}, \quad \alpha_0 \leq \frac{C_l}{LC_u^2}, \quad \eta \in [0.5, 1) \quad (81)$$

the sequence generated by

$$x_{t+1} = x_t - \alpha_t A_t g_t \quad (82)$$

satisfies

$$\frac{1}{T} \sum_{t=1}^T \|\nabla f(x_t)\|^2 \leq \frac{2}{C_l} \left[(M_f - f^*) \alpha_0 T^{\eta-1} + \frac{LC_u^2 \sigma^2 \alpha_0}{2(1-\eta)} T^{-\eta} \right] \quad (83)$$

where C_l and C_u are scalars representing the lower and upper bound for A_t , e.g. $C_l I \preceq A_t \preceq C_u I$, where $A \preceq B$ represents $B - A$ is semi-positive-definite.

Proof. Let

$$\delta_t = g_t - \nabla f(x_t) \quad (84)$$

then by **A.2**, $\mathbb{E}\delta_t = 0$.

$$f(x_{t+1}) \leq f(x_t) + \langle \nabla f(x_t), x_{t+1} - x_t \rangle + \frac{L}{2} \|x_{t+1} - x_t\|^2 \quad (85)$$

(by L -smoothness of $f(x)$)

$$= f(x_t) - \alpha_t \langle \nabla f(x_t), A_t g_t \rangle + \frac{L}{2} \alpha_t^2 \|A_t g_t\|^2 \quad (86)$$

$$= f(x_t) - \alpha_t \langle \nabla f(x_t), A_t (\delta_t + \nabla f(x_t)) \rangle + \frac{L}{2} \alpha_t^2 \|A_t g_t\|^2 \quad (87)$$

$$\leq f(x_t) - \alpha_t \langle \nabla f(x_t), A_t \nabla f(x_t) \rangle - \alpha_t \langle \nabla f(x_t), A_t \delta_t \rangle + \frac{L}{2} \alpha_t^2 C_u^2 \|g_t\|^2 \quad (88)$$

Take expectation on both sides of Eq. (88), conditioned on $\xi_{[t-1]} = \{x_1, x_2, \dots, x_{t-1}\}$, also notice that A_t is a constant given $\xi_{[t-1]}$, we have

$$\mathbb{E}[f(x_{t+1}) | x_1, \dots, x_t] \leq f(x_t) - \alpha_t \langle \nabla f(x_t), A_t \nabla f(x_t) \rangle + \frac{L}{2} \alpha_t^2 C_u^2 \mathbb{E} \|g_t\|^2 \quad (89)$$

(A_t is independent of g_t given $\{x_1, \dots, x_{t-1}\}$, and $\mathbb{E}\delta_t = 0$)

In order to bound RHS of Eq. (89), we first bound $\mathbb{E}[\|g_t\|^2]$.

$$\mathbb{E}[\|g_t\|^2 | x_1, \dots, x_t] = \mathbb{E}[\|\nabla f(x_t) + \delta_t\|^2 | x_1, \dots, x_t] \quad (90)$$

$$= \mathbb{E}[\|\nabla f(x_t)\|^2 | x_1, \dots, x_t] + \mathbb{E}[\|\nabla \delta_t\|^2 | x_1, \dots, x_t] + 2\mathbb{E}[\langle \delta_t, \nabla f(x_t) \rangle | x_1, \dots, x_t] \quad (91)$$

$$\leq \|\nabla f(x_t)\|^2 + \sigma^2 \quad (92)$$

(By **A.2**, and $\nabla f(x_t)$ is a constant given x_t)

Plug Eq. (92) into Eq. (89), we have

$$\mathbb{E}[f(x_{t+1}) | x_1, \dots, x_t] \leq f(x_t) - \alpha_t \langle \nabla f(x_t), A_t \nabla f(x_t) \rangle + \frac{L}{2} C_u^2 \alpha_t^2 [\|\nabla f(x_t)\|^2 + \sigma^2] \quad (93)$$

$$= f(x_t) - \left(\alpha_t C_l - \frac{L C_u^2 \alpha_t^2}{2} \right) \|\nabla f(x_t)\|^2 + \frac{L C_u^2 \sigma^2}{2} \alpha_t^2 \quad (94)$$

By **A.5** that $0 < \alpha_t \leq \frac{C_l}{L C_u^2}$, we have

$$\alpha_t C_l - \frac{L C_u^2 \alpha_t^2}{2} = \alpha_t \left(C_l - \frac{L C_u^2 \alpha_t}{2} \right) \geq \alpha_t \frac{C_l}{2} \quad (95)$$

Combine Eq. (94) and Eq. (95), we have

$$\frac{\alpha_t C_l}{2} \|\nabla f(x_t)\|^2 \leq \left(\alpha_t C_l - \frac{L C_u^2 \alpha_t^2}{2} \right) \|\nabla f(x_t)\|^2 \quad (96)$$

$$\leq f(x_t) - \mathbb{E}[f(x_{t+1}) | x_1, \dots, x_t] + \frac{L C_u^2 \sigma^2}{2} \alpha_t^2 \quad (97)$$

Then we have

$$\frac{C_l}{2} \|\nabla f(x_t)\|^2 \leq \frac{1}{\alpha_t} f(x_t) - \frac{1}{\alpha_t} \mathbb{E}[f(x_{t+1}) | x_1, \dots, x_t] + \frac{L C_u^2 \sigma^2}{2} \alpha_t \quad (98)$$

Perform telescope sum on Eq. (98), and recursively taking conditional expectations on the history of $\{x_i\}_{i=1}^T$, we have

$$\frac{C_l}{2} \sum_{t=1}^T \|\nabla f(x_t)\|^2 \leq \sum_{t=1}^T \frac{1}{\alpha_t} (\mathbb{E}f(x_t) - \mathbb{E}f(x_{t+1})) + \frac{L C_u^2 \sigma^2}{2} \sum_{t=1}^T \alpha_t \quad (99)$$

$$= \frac{\mathbb{E}f(x_1)}{\alpha_1} - \frac{\mathbb{E}f(x_{T+1})}{\alpha_T} + \sum_{t=2}^T \left(\frac{1}{\alpha_t} - \frac{1}{\alpha_{t-1}} \right) \mathbb{E}f(x_t) + \frac{L C_u^2 \sigma^2}{2} \sum_{t=1}^T \alpha_t \quad (100)$$

$$\leq \frac{M_f}{\alpha_1} - \frac{f^*}{\alpha_T} + M_f \sum_{t=1}^T \left(\frac{1}{\alpha_t} - \frac{1}{\alpha_{t-1}} \right) + \frac{L C_u^2 \sigma^2}{2} \sum_{t=1}^T \alpha_t \quad (101)$$

$$\leq \frac{M_f - f^*}{\alpha_T} + \frac{L C_u^2 \sigma^2}{2} \sum_{t=1}^T \alpha_t \quad (102)$$

$$\leq (M_f - f^*) \alpha_0 T^\eta + \frac{L C_u^2 \sigma^2 \alpha_0}{2} \left(\zeta(\eta) + \frac{T^{1-\eta}}{1-\eta} + \frac{1}{2} T^{-\eta} \right) \quad (103)$$

(By sum of generalized harmonic series,

$$\sum_{k=1}^n \frac{1}{k^s} \sim \zeta(s) + \frac{n^{1-s}}{1-s} + \frac{1}{2n^s} + O(n^{-s-1}), \quad (104)$$

$\zeta(s)$ is Riemann zeta function.)

Then we have

$$\frac{1}{T} \sum_{t=1}^T \left\| \nabla f(x_t) \right\|^2 \leq \frac{2}{C_l} \left[(M_f - f^*) \alpha_0 T^{\eta-1} + \frac{LC_u^2 \sigma^2 \alpha_0}{2(1-\eta)} T^{-\eta} \right] \quad (105)$$

□

B.2.1 Validation on numerical accuracy of sum of generalized harmonic series

We performed experiments to test the accuracy of the analytical expression of sum of harmonic series. We numerically calculate $\sum_{i=1}^N \frac{1}{i^\eta}$ for η varying from 0.5 to 0.999, and for N ranging from 10^3 to 10^7 in the log-grid. We calculate the error of the analytical expression by Eq. (104), and plot the error in Fig. 21. Note that the y -axis has a unit of 10^{-7} , while the sum is typically on the order of 10^3 , this implies that expression Eq. (104) is very accurate and the relative error is on the order of 10^{-10} . Furthermore, note that this expression is accurate even when $\eta = 0.5$.

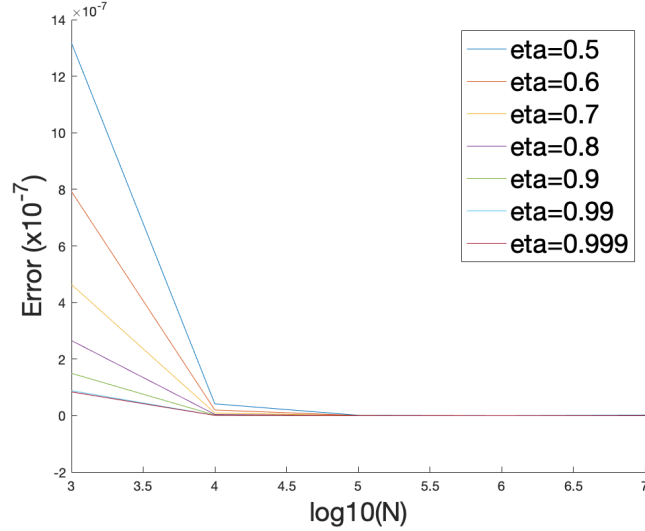


Figure 21: The error between numerical sum for $\sum_{i=1}^N \frac{1}{i^\eta}$ and the analytical form.

B.3 Convergence analysis of Async-moment-optimizers in stochastic non-convex optimization

Lemma B.2. Let $m_t = \beta_1 m_{t-1} + (1 - \beta_1) g_t$, let $A_t \in \mathbb{R}^d$, then

$$\langle A_t, g_t \rangle = \frac{1}{1 - \beta_1} \left(\langle A_t, m_t \rangle - \langle A_{t-1}, m_{t-1} \rangle \right) + \langle A_{t-1}, m_{t-1} \rangle + \frac{\beta_1}{1 - \beta_1} \langle A_{t-1} - A_t, m_{t-1} \rangle \quad (106)$$

Theorem B.3. Under assumptions 1-4, $\beta_1 < 1, \beta_2 < 1$, also assume $A_{t+1} \leq A_t$ element-wise which can be achieved by tracking maximum of s_t as in AMSGrad, f is upper bounded by M_f , $\|g_t\|_\infty \leq M_g$, with learning rate schedule as

$$\alpha_t = \alpha_0 t^{-\eta}, \quad \alpha_0 \leq \frac{C_l}{LC_u^2}, \quad \eta \in (0.5, 1] \quad (107)$$

the sequence is generated by

$$x_{t+1} = x_t - \alpha_t A_t m_t \quad (108)$$

then we have

$$\frac{1}{T} \sum_{t=1}^T \left\| \nabla f(x_t) \right\|^2 \leq \frac{1}{\alpha_0 C_l} T^{\eta-1} \left[M_f - f^* + E M_g^2 \right] \quad (109)$$

where

$$E = \frac{\beta_1^2}{4L(1-\beta_1)^2} + \frac{1}{1-\beta_1} \alpha_0 M_g + \left(\frac{\beta_1}{1-\beta_1} + \frac{1}{2} \right) L \alpha_0^2 C_u^2 \frac{1}{1-2\eta} \quad (110)$$

Proof. Let $A_t = \alpha_t A_t \nabla f(x_t)$ and let $A_0 = A_1$, we have

$$\sum_{t=1}^T \langle A_t, g_t \rangle = \frac{1}{1-\beta_1} \langle A_T, m_T \rangle + \sum_{t=1}^T \langle A_{t-1}, m_{t-1} \rangle + \frac{\beta_1}{1-\beta_1} \sum_{t=1}^T \langle A_{t-1} - A_t, m_{t-1} \rangle \quad (111)$$

$$= \frac{\beta_1}{1-\beta_1} \langle A_T, m_T \rangle + \sum_{t=1}^T \langle A_t, m_t \rangle + \frac{\beta_1}{1-\beta_1} \sum_{t=0}^{T-1} \langle A_t - A_{t+1}, m_t \rangle \quad (112)$$

First we derive a lower bound for Eq. (112).

$$\langle A_t, g_t \rangle = \langle \alpha_t A_t \nabla f(x_t), g_t \rangle \quad (113)$$

$$= \langle \alpha_t A_t \nabla f(x_t) - \alpha_{t-1} A_{t-1} \nabla f(x_t), g_t \rangle + \langle \alpha_{t-1} A_{t-1} \nabla f(x_t), g_t \rangle \quad (114)$$

$$= \langle \alpha_{t-1} A_{t-1} \nabla f(x_t), g_t \rangle - \langle (\alpha_{t-1} A_{t-1} - \alpha_t A_t) \nabla f(x_t), g_t \rangle \quad (115)$$

$$\geq \langle \alpha_{t-1} A_{t-1} \nabla f(x_t), g_t \rangle - \left\| \nabla f(x_t) \right\|_{\infty} \left\| \alpha_{t-1} A_{t-1} - \alpha_t A_t \right\|_1 \left\| g_t \right\|_{\infty} \quad (116)$$

(By Hölder's inequality)

$$\geq \langle \alpha_{t-1} A_{t-1} \nabla f(x_t), g_t \rangle - M_g^2 \left(\left\| \alpha_{t-1} A_{t-1} \right\|_1 - \left\| \alpha_t A_t \right\|_1 \right) \quad (117)$$

$$\left(\text{Since } \left\| g_t \right\|_{\infty} \leq M_g, \alpha_{t-1} \geq \alpha_t > 0, A_{t-1} \geq A_t > 0 \text{ element-wise} \right) \quad (118)$$

Perform telescope sum, we have

$$\sum_{t=1}^T \langle A_t, g_t \rangle \geq \sum_{t=1}^T \langle \alpha_{t-1} A_{t-1} \nabla f(x_t), g_t \rangle - M_g^2 \left(\left\| \alpha_0 H_0 \right\|_1 - \left\| \alpha_T A_T \right\|_1 \right) \quad (119)$$

Next, we derive an upper bound for $\sum_{t=1}^T \langle A_t, g_t \rangle$ by deriving an upper-bound for the RHS of Eq. (112). We derive an upper bound for each part.

$$\langle A_t, m_t \rangle = \langle \alpha_t A_t \nabla f(x_t), m_t \rangle = \langle \nabla f(x_t), \alpha_t A_t m_t \rangle \quad (120)$$

$$= \langle \nabla f(x_t), x_t - x_{t+1} \rangle \quad (121)$$

$$\leq f(x_t) - f(x_{t+1}) + \frac{L}{2} \left\| x_{t+1} - x_t \right\|^2 \left(\text{By } L\text{-smoothness of } f \right) \quad (122)$$

Perform telescope sum, we have

$$\sum_{t=1}^T \langle A_t, m_t \rangle \leq f(x_1) - f(x_{T+1}) + \frac{L}{2} \sum_{t=1}^T \left\| \alpha_t A_t m_t \right\|^2 \quad (123)$$

$$\langle A_t - A_{t+1}, m_t \rangle = \langle \alpha_t A_t \nabla f(x_t) - \alpha_{t+1} A_{t+1} \nabla f(x_{t+1}), m_t \rangle \quad (124)$$

$$= \langle \alpha_t A_t \nabla f(x_t) - \alpha_t A_t \nabla f(x_{t+1}), m_t \rangle$$

$$+ \langle \alpha_t A_t \nabla f(x_{t+1}) - \alpha_{t+1} A_{t+1} \nabla f(x_{t+1}), m_t \rangle \quad (125)$$

$$= \langle \nabla f(x_t) - \nabla f(x_{t+1}), \alpha_t A_t m_t \rangle + \langle (\alpha_t A_t - \alpha_{t+1} A_{t+1}) \nabla f(x_t), m_t \rangle \quad (126)$$

$$= \langle \nabla f(x_t) - \nabla f(x_{t+1}), x_t - x_{t+1} \rangle + \langle \nabla f(x_t), (\alpha_t A_t - \alpha_{t+1} A_{t+1}) m_t \rangle \quad (127)$$

$$\leq L \|x_{t+1} - x_t\|^2 + \langle \nabla f(x_t), (\alpha_t A_t - \alpha_{t+1} A_{t+1}) m_t \rangle \quad (128)$$

(By smoothness of f)

$$\leq L \|x_{t+1} - x_t\|^2 + \|\nabla f(x_t)\|_\infty \|\alpha_t A_t - \alpha_{t+1} A_{t+1}\|_1 \|m_t\|_\infty \quad (129)$$

(By Hölder's inequality)

$$\leq L \|x_{t+1} - x_t\|^2 + M_g^2 \left(\|\alpha_t A_t\|_1 - \|\alpha_{t+1} A_{t+1}\|_1 \right) \quad (130)$$

$$\left(\text{Since } \alpha_t \geq \alpha_{t+1} \geq 0, A_t \geq A_{t+1} \geq 0, \text{ element-wise} \right) \quad (131)$$

Perform telescope sum, we have

$$\sum_{t=1}^{T-1} \langle A_t - A_{t+1}, m_t \rangle \leq L \sum_{t=1}^{T-1} \|\alpha_t A_t m_t\|^2 + M_g^2 \left(\|\alpha_1 H_1\|_1 - \|\alpha_T A_t\|_1 \right) \quad (132)$$

We also have

$$\langle A_T, m_T \rangle = \langle \alpha_T A_T \nabla f(x_T), m_T \rangle = \langle \nabla f(x_T), \alpha_T A_T m_T \rangle \quad (133)$$

$$\leq L \frac{1 - \beta_1}{\beta_1} \|\alpha_T A_T m_T\|^2 + \frac{\beta_1}{4L(1 - \beta_1)} \|\nabla f(x_T)\|^2 \quad (134)$$

(By Young's inequality)

$$= L \frac{1 - \beta_1}{\beta_1} \|\alpha_T A_T m_T\|^2 + \frac{\beta_1}{4L(1 - \beta_1)} M_g^2 \quad (135)$$

Combine Eq. (123), Eq. (132) and Eq. (135) into Eq. (112), we have

$$\begin{aligned} \sum_{t=1}^T \langle A_t, g_t \rangle &\leq \frac{\beta_1}{1 - \beta_1} \langle A_T, m_T \rangle + f(x_1) - f(x_{T+1}) + \frac{L}{2} \sum_{t=1}^T \|\alpha_t A_t m_t\|^2 \\ &\quad + \frac{\beta_1}{1 - \beta_1} L \sum_{t=1}^{T-1} \|\alpha_t A_t m_t\|^2 + \frac{\beta_1}{1 - \beta_1} M_g^2 \left(\|\alpha_1 H_1\|_1 - \|\alpha_T A_t\|_1 \right) \end{aligned} \quad (136)$$

$$\begin{aligned} &\leq f(x_1) - f(x_{T+1}) + \left(\frac{\beta_1}{1 - \beta_1} + \frac{1}{2} \right) L \sum_{t=1}^T \|\alpha_t A_t m_t\|^2 \\ &\quad + \left(\frac{\beta_1^2}{4L(1 - \beta_1)^2} + \frac{\beta_1}{1 - \beta_1} \|\alpha_1 H_1\|_1 \right) M_g^2 \end{aligned} \quad (137)$$

Combine Eq. (119) and Eq. (137), we have

$$\begin{aligned} \sum_{t=1}^T \langle \alpha_{t-1} A_{t-1} \nabla f(x_t), g_t \rangle - M_g^2 \left(\|\alpha_0 H_0\|_1 - \|\alpha_T A_t\|_1 \right) &\leq \sum_{t=1}^T \langle A_t, g_t \rangle \\ &\leq f(x_1) - f(x_{T+1}) + \left(\frac{\beta_1}{1 - \beta_1} + \frac{1}{2} \right) L \sum_{t=1}^T \|\alpha_t A_t m_t\|^2 \\ &\quad + \left(\frac{\beta_1^2}{4L(1 - \beta_1)^2} + \frac{\beta_1}{1 - \beta_1} \|\alpha_1 H_1\|_1 \right) M_g^2 \end{aligned} \quad (138)$$

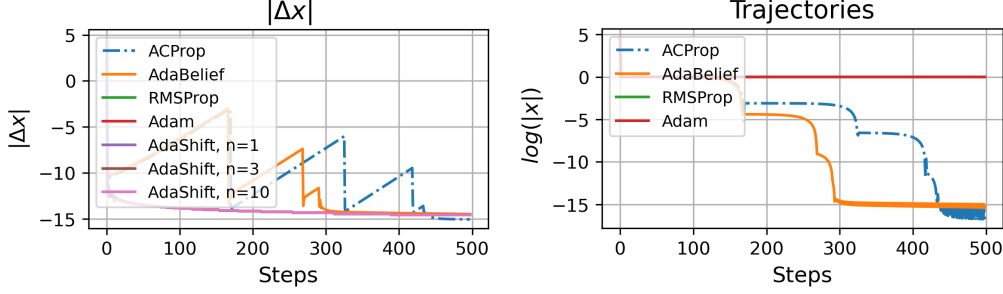


Figure 22: Behavior of ACProp for optimization of the function $f(x) = |x|$ with $lr = 0.00001$.

Hence we have

$$\begin{aligned} \sum_{t=1}^T \langle \alpha_{t-1} A_{t-1} \nabla f(x_t), g_t \rangle &\leq f(x_1) - f(x_{T+1}) + \left(\frac{\beta_1}{1-\beta_1} + \frac{1}{2} \right) L \sum_{t=1}^T \|\alpha_t A_t m_t\|^2 \\ &+ \left(\frac{\beta_1^2}{4L(1-\beta_1)^2} + \|\alpha_0 H_0\|_1 + \frac{\beta_1}{1-\beta_1} \|\alpha_1 H_1\|_1 \right) M_g^2 \end{aligned} \quad (139)$$

$$\begin{aligned} &\leq f(x_1) - f^* + \left(\frac{\beta_1}{1-\beta_1} + \frac{1}{2} \right) L \alpha_0^2 M_g^2 C_u^2 \sum_{t=1}^T t^{-2\eta} \\ &+ \left(\frac{\beta_1^2}{4L(1-\beta_1)^2} + \|\alpha_0 H_0\|_1 + \frac{\beta_1}{1-\beta_1} \|\alpha_1 H_1\|_1 \right) M_g^2 \end{aligned} \quad (140)$$

$$\begin{aligned} &\leq f(x_1) - f^* \\ &+ M_g^2 \left[\frac{\beta_1^2}{4L(1-\beta_1)^2} + \|\alpha_0 H_0\|_1 + \frac{\beta_1}{1-\beta_1} \|\alpha_1 H_1\|_1 + \left(\frac{\beta_1}{1-\beta_1} + \frac{1}{2} \right) L \alpha_0^2 C_u^2 \frac{T^{1-2\eta}}{1-2\eta} \right] \end{aligned} \quad (141)$$

$$\begin{aligned} &\leq f(x_1) - f^* + M_g^2 \underbrace{\left[\frac{\beta_1^2}{4L(1-\beta_1)^2} + \frac{1}{1-\beta_1} \alpha_0 M_g + \left(\frac{\beta_1}{1-\beta_1} + \frac{1}{2} \right) L \alpha_0^2 C_u^2 \frac{1}{1-2\eta} \right]}_E \end{aligned} \quad (142)$$

Take expectations on both sides, we have

$$\sum_{t=1}^T \langle \alpha_{t-1} A_{t-1} \nabla f(x_t), \nabla f(x_t) \rangle \leq \mathbb{E} f(x_1) - f^* + E M_g^2 \leq M_f - f^* + E M_g^2 \quad (143)$$

Note that we have α_t decays monotonically with t , hence

$$\sum_{t=1}^T \langle \alpha_{t-1} A_{t-1} \nabla f(x_t), \nabla f(x_t) \rangle \geq \alpha_0 T^{-\eta} \sum_{t=1}^T \langle A_{t-1} \nabla f(x_t), \nabla f(x_t) \rangle \quad (144)$$

$$\geq \alpha_0 T^{1-\eta} C_l \left[\frac{1}{T} \sum_{t=1}^T \|\nabla f(x_t)\|^2 \right] \quad (145)$$

Combine Eq. (143) and Eq. (145), assume f is upper bounded by M_f , we have

$$\frac{1}{T} \sum_{t=1}^T \|\nabla f(x_t)\|^2 \leq \frac{1}{\alpha_0 C_l} T^{\eta-1} [M_f - f^* + E M_g^2] \quad (146)$$

□

C Experiments

C.1 Centering of second momentum does not suffer from numerical issues

Note that the centered second momentum s_t does not suffer from numerical issues in practice. The intuition that “ s_t is an estimate of variance in gradient” is based on a strong assumption that the

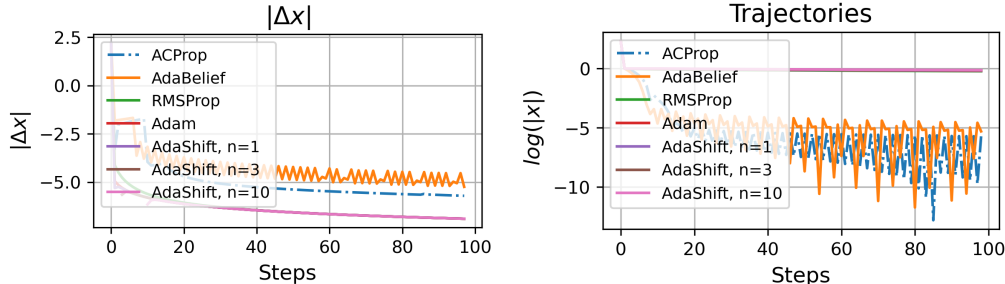


Figure 23: Behavior of ACProp for optimization of the function $f(x) = |x|$ with $lr = 0.01$.

Table 6: Hyper-parameters for ACProp in various experiments

	lr	beta1	beta2	eps
ImageNet	1e-3	0.9	0.999	1e-12
GAN	2e-4	0.5	0.999	1e-16
Transformer	5e-4	0.9	0.999	1e-16

gradient follows a stationary distribution, which indicates that the true gradient $\nabla f_t(x)$ remains a constant function of t . In fact, s_t tracks $EMA((g_t - m_t)^2)$, and it includes two aspects: the change in true gradient $\|\nabla f_{t+1}(x) - \nabla f_t(x)\|^2$, and the noise in gradient observation $\|g_t - \nabla f_t(x)\|^2$. In practice, especially in deep learning, the gradient suffers from large noise, hence s_t does not take extremely small values.

Next, we consider an ideal case that the observation g_t is noiseless, and conduct experiments to show that centering of second-momentum does not suffer from numerical issues. Consider the function $f(x) = |x|$ with initial value $x_0 = 100$, we plot the trajectories and stepsizes of various optimizers in Fig. 22 and Fig. 23 with initial learning rate $lr = 0.00001$ and $lr = 0.01$ respectively. Note that ACProp and AdaBelief take a large step at the initial phase, because a constant gradient is observed without noise. But note that the gradient remains constant only within half of the plane; when it cross the boundary $x = 0$, the gradient is reversed, hence $\|\nabla f_{t+1}(x) - \nabla f_t(x)\|^2 \neq 0$, and s_t becomes a non-zero value when it hits a valley in the loss surface. Therefore, the stepsize of ACProp and AdaBelief automatically decreases when they reach the local minimum. As shown in Fig. 22 and Fig. 23, ACProp and AdaBelief does not take any extremely large stepsizes for both a very large (0.01) and very small (0.00001) learning rates, and they automatically decrease stepsizes near the optimal. We do not observe any numerical issues even for noise-free piecewise-linear functions. If the function is not piecewise linear, or the gradient does not remain constant within any connected set, then $\|\nabla f_{t+1}(x) - \nabla f_t(x)\|^2 \neq 0$ almost everywhere, and the numerical issue will never happen.

The only possible case where centering second momentum causes numerical issue has to satisfy two conditions simultaneously: (1) $\|\nabla f_{t+1}(x) - \nabla f_t(x)\|^2 = 0, \forall t$ and (2) g_t is a noise-free observation of $\nabla f(x)$. This is a trivial case where the loss surface is linear, and gradient is noise-free. This is case is almost never encountered in practice. Furthermore, in this case, $s_t = 0$ and ACProp reduces to SGD with stepsize $1/\epsilon$. But note that the optimal is $-\infty$ and achieved at ∞ or $-\infty$, taking a large stepsize $1/\epsilon$ is still acceptable for this trivial case.

C.2 Image classification with CNN

We performed extensive hyper-parameter tuning in order to better compare the performance of different optimizers: for SGD we set the momentum as 0.9 which is the default for many cases, and search the learning rate between 0.1 and 10^{-5} in the log-grid; for other adaptive optimizers, including AdaBelief, Adam, RAdam, AdamW and AdaShift, we search the learning rate between 0.01 and 10^{-5} in the log-grid, and search ϵ between 10^{-5} and 10^{-10} in the log-grid. We use a weight decay of 5e-2 for AdamW, and use 5e-4 for other optimizers. We conducted experiments based on the official code for AdaBound and AdaBelief ¹.

¹<https://github.com/juntang-zhuang/Adabelief-Optimizer>

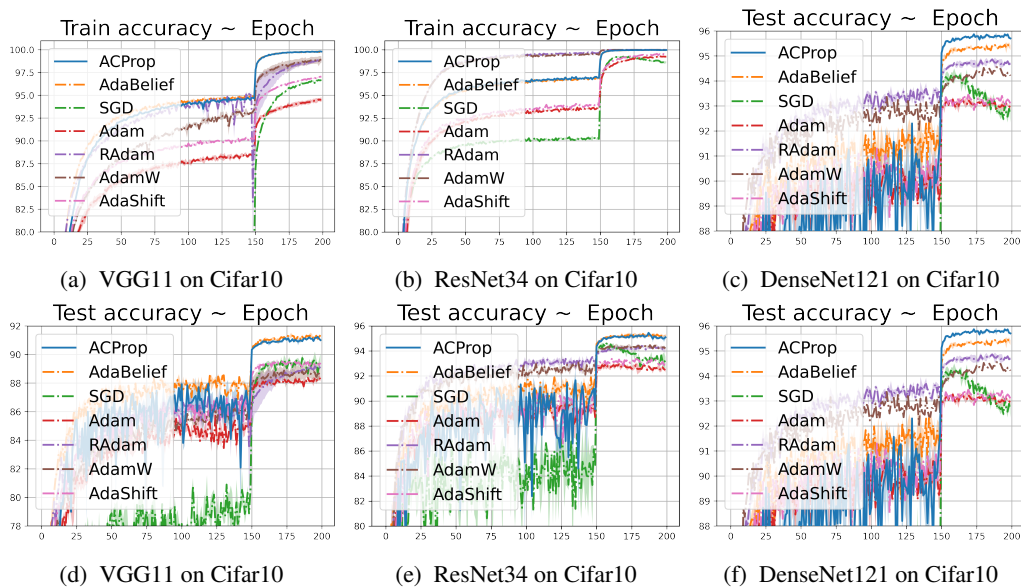


Figure 24: Training (top row) and test (bottom row) accuracy of CNNs on Cifar10 dataset.

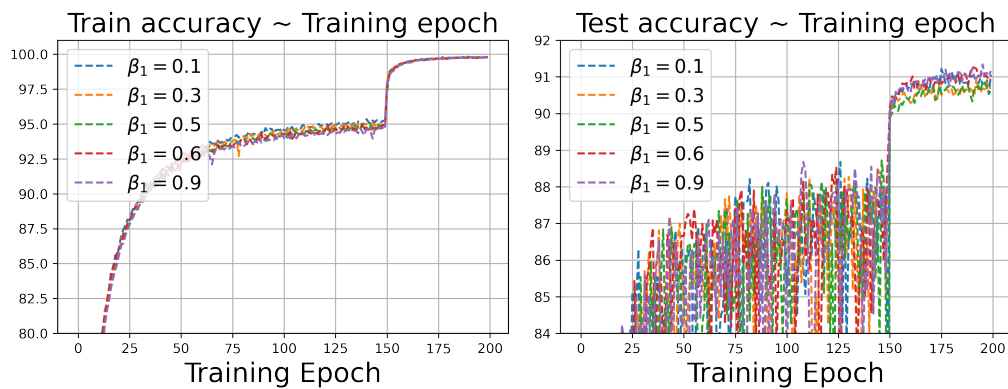


Figure 26: The training and test accuracy curve of VGG11 on CIFAR10 with different β_1 values.

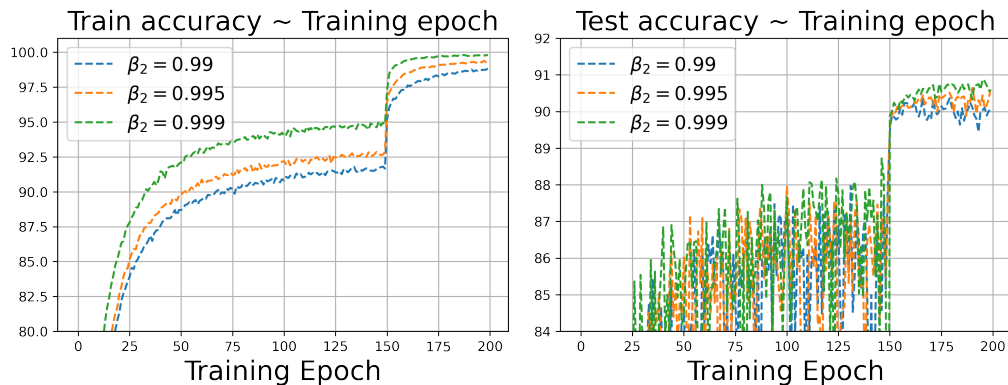


Figure 28: The training and test accuracy curve of VGG11 on CIFAR10 with different β_2 values.

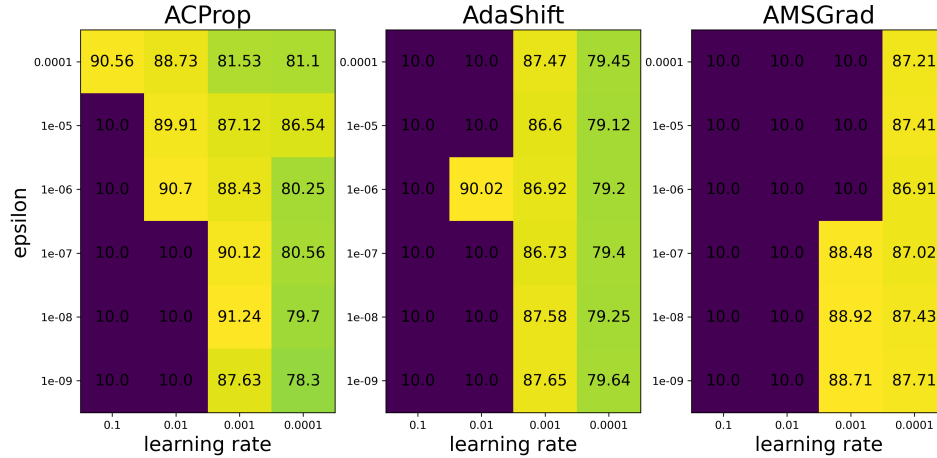


Figure 29: Test accuracy of VGG-11 on CIFAR10 trained under various hyper-parameter settings with different optimizers

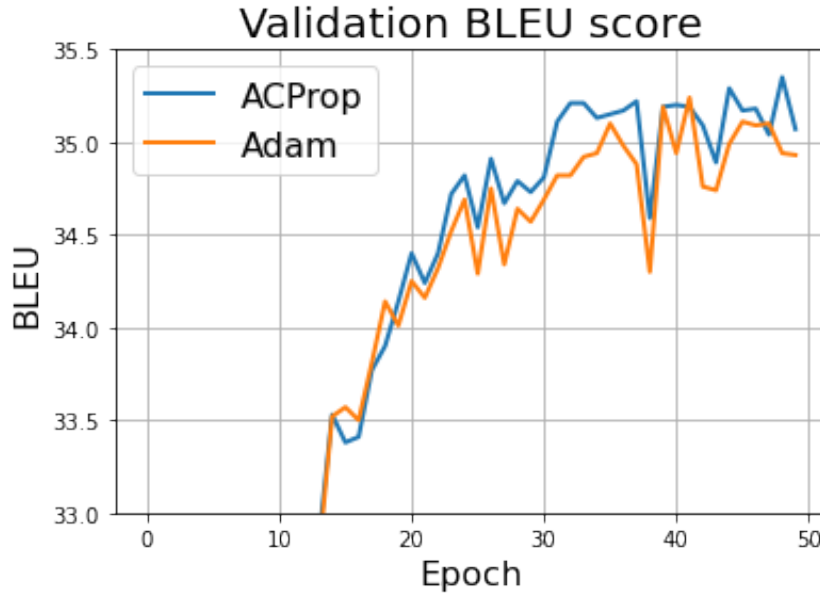


Figure 30: BLEU score on validation set of a Transformer-base trained with ACProp and Adam

We further test the robustness of ACProp to values of hyper-parameters β_1 and β_2 . Results are shown in Fig. 26 and Fig. 28 respectively. ACProp is robust to different values of β_1 , and is more sensitive to values of β_2 .

C.3 Neural Machine Translation with Transformers

We conducted experiments on Neural Machine Translation (NMT) with transformer models. Our experiments on the IWSLT14 DE-EN task is based on the 6-layer transformer-base model in fairseq implementation². For all methods, we use a learning rate of 0.0002, and standard invser sqrt learning rate schedule with 4,000 steps of warmup. For other tasks, our experiments are based on an open-source implementation³ using a 1-layer Transformer model. We plot the BLEU score on validation

²<https://github.com/pytorch/fairseq>

³https://github.com/DevSinghSachan/multilingual_nmt

set varying with training epoch in Fig. 30, and ACProp consistently outperforms Adam throughout the training.

C.4 Generative adversarial networks

The training of GANs easily suffers from mode collapse and numerical instability [34], hence is a good test for the stability of optimizers. We conducted experiments with Deep Convolutional GAN (DCGAN) [35], Spectral-Norm GAN (SNGAN) [36], Self-Attention GAN (SAGAN) [37] and Relativistic-GAN (RLGAN) [38]. We set $\beta_1 = 0.5$, and search for β_2 and ϵ with the same schedule as previous section. Our experiments are based on an open-source implementation ⁴.

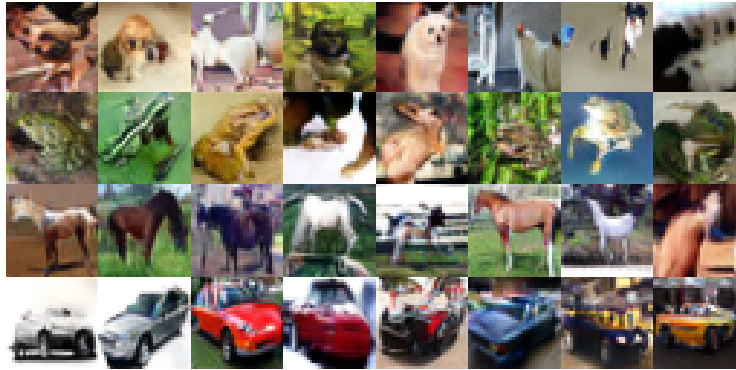


Figure 31: Generated figures by the SN-GAN trained with ACProp.

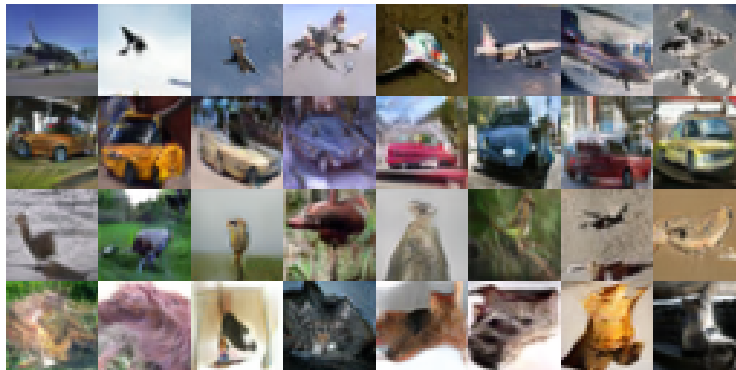


Figure 32: Generated figures by the SA-GAN trained with ACProp.

⁴<https://github.com/POSTECH-CVLab/PyTorch-StudioGAN>

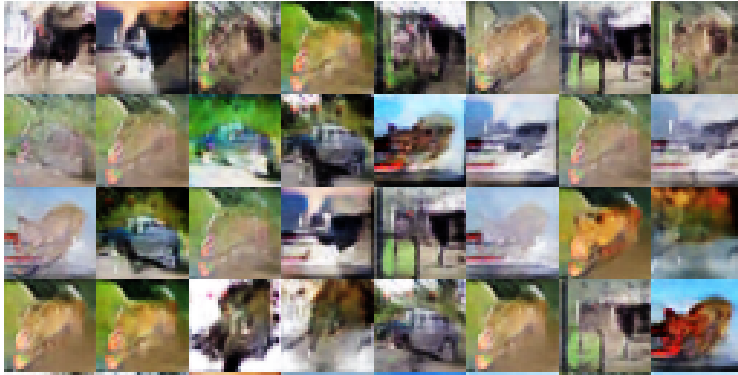


Figure 33: Generated figures by the DC-GAN trained with ACProp.

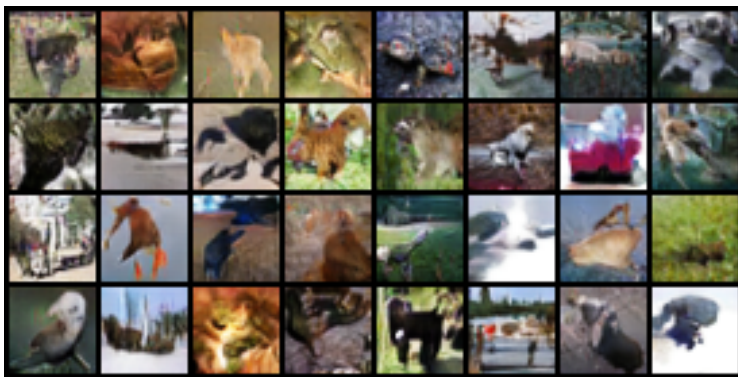


Figure 34: Generated figures by the RL-GAN trained with ACProp.